HHS Public Access

Author manuscript

Int J Min Sci Technol. Author manuscript; available in PMC 2019 January 24.

Published in final edited form as:

Int J Min Sci Technol. 2018 January ; 28(1): 85–93. doi:10.1016/j.ijmst.2017.11.012.

Deep cover bleeder entry performance and support loading: A case study

Ted M. Klemetti[a,*], **Mark Alexander Van Dyke**[a], and **Ihsan Berk Tulu**[b]

[a]Ground Control Branch, NIOSH, Pittsburgh Mining Research Division, Pittsburgh 15236, USA

[b]Mining Engineering Department, West Virginia University, Morgantown 26505, USA

Abstract

Several questions have emerged in relation to deep cover bleeder entry performance and support loading: how well do current modeling procedures calculate the rear abutment extent and loading? Does an improved understanding of the rear abutment extent warrant a change in standing support in bleeder entries? To help answer these questions and to determine the current utilization of standing support in bleeder entries, four bleeder entries at varying distances from the startup room were instrumented, observed, and numerically modeled. This paper details observations made by NIOSH researchers in the bleeder entries of a deep cover longwall panel—specifically data collected from instrumented pumpable cribs, observations of the conditions of the entries, and numerical modeling of the bleeder entries during longwall extraction. The primary focus was on the extent and magnitude of the abutment loading experienced by the standing support. As expected, the instrumentation of the standing supports showed very little loading relative to the capacity of the standing supports—less than 23 Mg load and 2.54 cm convergence. The Flac3D program was used to evaluate these four bleeder entries using previously defined modeling and input parameter estimation procedures. The results indicated only a minor increase in load during the extraction of the longwall panel. The model showed a much greater increase in stress due to the development of the gateroad and bleeder entries, with about 80% of the increase associated with development and 20% with longwall extraction. The Flac3D model showed very good correlation between expected gateroad loading during panel extraction and that expected based on previous studies. The results of this study showed that the rear abutment stress experienced by this bleeder entry design was minimal. The farther away from the startup room, the lower the applied load and smaller the convergence in the entry if all else is held constant. Finally, the numerical modeling method used in this study was capable of replicating the expected and measured results near seam.

Keywords

Bleeder entry; Standing supports; Abutment loading; Longwall mining; Full extraction

*Corresponding author. TKlemetti@cdc.gov (T.M. Klemetti).

1. Introduction

The National Institute for Occupational Safety and Health (NIOSH) recently began a research project aimed at improving understanding of stress redistribution due to full extraction mining and the methodologies to assess those stresses in underground coal mining. Two methods of mining coal are of primary interest to this project: longwall and room-and-pillar retreat. This paper focuses on the stress redistribution due to longwall mining.

Fig. 1 shows a longwall mine layout containing two gateroads, the longwall panel, startup room, and the bleeder entries. The longwall face and shields are initially located in the startup room and they progress towards the recovery room at the opposite end of the longwall panel. Once the shields begin moving towards the recovery room, the area mined out behind the shields becomes the gob—the broken overburden that fills the void created by the longwall mining process. The overburden stress after longwall mining is redistributed among the longwall panel outby the face, the shields in the face, the gob behind the shields, the gateroads on either side of the panel, and the bleeder pillars behind the gob. Fig. 1 shows a barrier pillar between the startup room and the bleeder entries that can also accept the load previously carried by the pre-mining longwall panel.

The bleeder pillars, entries, and standing support were studied in this research effort because they provide support to the bleeder entries that need to be accessible, and they provide ventilation support to the current and future longwall panels. In the past, load redistribution has been studied with a focus on the gateroads, longwall face, and, occasionally, the recovery rooms. Recovery rooms are the area at the end of the longwall panel where the face equipment is recovered for use in the subsequent longwall panel. Most of the recovery rooms studied in the past were pre-driven recovery rooms where the enlarged opening, around 7.6 m, was mined and supported prior to the longwall face reaching the recovery area. The redistributed load is referred to as the abutment— specifically, the front abutment, side abutment, and rear abutment (gob loading). The results of these previous studies show that the abutment extents and magnitudes are variable and associated with depth of cover, overburden lithology and mechanical properties, and mining sequence [1,2]. Hill, Stone, Suchowerska, and Trueman provide case studies that show abutment extent and magnitude are impacted by the specific mine, as well as the location of the abutment loading [2]. Peng links the maximum front abutment load to geologic conditions, face position relative to entry setup and periodic roof weighting, and adjacent mined-out areas [1]. A more streamlined approach to determining pillar stability, load redistribution, and abutment extent and magnitude uses a constant abutment angle of 21° and can be found in ALPS and ARMPS [3,4].

Bleeder support evaluations and designs primarily rely on experience at specific locations. Two recent studies address the bleeder support issue through numerical modeling simulations [5,6]. Although limited study has been given to bleeder supports, the same types of supports have been used elsewhere in mining and have been evaluated in those settings (for example, tailgate entry support, headgate entry support, and pre-driven recovery rooms). The tailgate study conducted by Zhang et al. in 2012 shows the importance of fairly high

yield strengths while maintaining a reasonable residual strength through extended convergence [6]. In the case presented by Zhang et al. in their 2012 publication, the mine was relatively shallow, and the measured convergence that the standing support must endure ranged from a minimum of 3.8 cm to a maximum of 20.4 cm [6]. In addition, a pre-driven longwall recovery room was studied where pumpable cribs were instrumented in the same manner as used in this study and compared to their laboratory performance and capacity [7]. This study showed that 5–10 cm of convergence indicated that standing support is necessary, although the study monitored front abutment loading rather than rear bleeder loading [7].

Campoli studied pumpable crib supports for use in longwall gateroads and bleeder entries [8]. Again, the focus was on gateroads more than on bleeders, and this study emphasized field experience and laboratory testing. The field experience demonstrates the success of a double row of 61- or 76-cm-diameter pumpable cribs in bleeder entries around the country [8]. Different size pumpable cribs are used, depending on the support capacity needs, width-to-height ratio, and entry width. Laboratory testing of pumpable cribs has been ongoing for the past 20-plus years. A study conducted by Batchler focused on the design characteristics of pumpable supports' effect on their performance [9]. Batchler's database includes over 160 tests during the preceding seven years and promotes the importance of the stiffness, peak load capacity, load shedding events, and residual load characteristics [9]. NIOSH developed a software program called support technology optimization program (STOP) to allow mine planners and designers to evaluate different support types under varying conditions [10,11].

All of these previous research efforts helped us to develop and design this research project and allowed us to focus on areas not studied in-depth previously. Some of the questions developed from the results of these previous studies are as follows: how well do current modeling procedures calculate the rear abutment extent and loading? does an improved understanding of the rear abutment extent warrant a change in standing support in bleeder entries? what is the optimal standing support for bleeder entries separated from the startup room by a barrier pillar?

To help answer these questions and to determine the current utilization of standing support in bleeder entries, four bleeder entries at varying distances from the startup room were instrumented, observed, and numerically modeled. This evaluation was intended to determine the rear abutment extent and magnitude at various locations to optimize standing support in these entries and in those under similar conditions.

2. Field investigation

2.1. Mine conditions

Fig. 2 shows the geometry of the study sites. The depth of cover throughout the mine ranges from 365 to 701 m. The longwall panels in the newer districts are 213 m wide and 3048–3505 m long. The gateroad comprises a yield-abutment-yield system with entry centers of 15, 52, and 15 m, respectively. The crosscut centers for the abutment pillars are 137 and are 45 m for the yield pillars. The mining height averages 2.3 m with a range from 1.5 to 3.7 m. There are mined-out seams above the current seam, although no multiple seam interactions are anticipated. The mine generally mines in "districts," consisting of 4–6 longwall panels

separated by a barrier pillar. The panels within a district use a common set of bleeder entries behind the startup rooms of the longwall panels. The bleeder entries consist of an entry 30.5 m directly behind the startup room, followed by a 91.5-m-wide barrier pillar. Then there is an additional set of four bleeder entries on 30.5-m centers with crosscut spacing varying from 38 to 52 m, as seen in Fig. 2.

Throughout the gateroads and bleeders, fully grouted torque-tension bolts on a 1.2-by-1.2-m pattern are installed with 3.7-m cable bolts installed in all intersections and as needed in the entries based on geological conditions. The standing support installed in the gateroads consists of a double row in the #2 and #1 entries. The bleeders have standing support installed in all four entries behind the barrier pillar, as well as the entry behind the startup room. The first two pillars have double rows of standing support on 1.8 and 2.4 m centers. The second two entries have six and four pumpable supports per intersection.

The geology of the 26-right panel consists of strata defined by cyclothems, an alternating repetitive sequence of sediments derived from marine and non-marine sources with coal beds in between the transitions from marine to non-marine sediment sequences (Fig. 3). The longwall mine operates within the Pocahontas Number 3 seam, known for its low sulfur and ash metallurgical grade coal. The Pocahontas Number 3 seam was deposited in an upper delta environment that resulted in thickly to massively bedded sandstones with a small series of shales lenses occurring occasionally. The geology in the floor of the seam consists of a fireclay that is approximately 15–61 cm thick, which acts as a sedimentary trap for thick and sometimes gas-laden sandstone below the fireclay. The floor sandstone is usually 4.6–9.2 m thick and is thinly bedded with coal and mica streaks, which makes it relatively weak compared to the roof sandstones.

The Pocahontas Number 3 seam is subject to drastic upper and lower partings that split from the main bench and separate a few meters from the main bench within a short span of a hundred meters. In the area of the bleeders of 26-right, the lower parting is just beginning to separate, and the parting is usually around 15 cm thick. However, the clay parting has caused the lower portion of the coal to be subject to minor folding, which causes the lower portion of the coal under the parting to spall at faster rates than the rest of the main bench. This condition creates a brow condition that could be subject to rib roll.

The geology above the seam consists of a silty dark shale that varies from 0 to 7.6 m thick in the immediate roof above the main bench. Above the shale, there is thinly to thickly bedded sandstone that contains few mica and coal streaks; the sandstone is approximately 0–10.7 m thick and is named sandstone 1 by the mine. Above the sandstone 1, there is a shale parting that is a maximum of 1.5 m thick and, at times, is not present. Above the shale parting there is another sandstone that, at times, can combine with the sandstone 1 if the shale parting is not present. This sandstone, named sandstone 2, is stronger and has thicker bedding, which is typically massive and is usually 7.6–10.7 m thick. The Pocahontas Number 4 seam is above the sandstone 2, and it is usually 0–61 cm thick and on average 15 m above the Pocahontas Number 3 seam.

2.2. Instrumentation site plan

The monitoring plan consisted of two phases: (1) instrumented standing supports and (2) visual observations. The instrumentation plan included five sites located within the study area, highlighted in Fig. 2. The instrumentation and initial visual observation were planned for immediately prior to the longwall panel beginning, or during the installation of the bleeder standing support. The timing of the installation did not capture any development or previous longwall panel loading on the bleeders, although the bleeder entry standing supports are traditionally not exposed to any of that loading. This plan allowed for actual observation and measurement of the as-planned standing support life. Because this was the final panel in a district, the effect of future panels on the bleeder entries of this panel cannot be monitored. In addition, scope holes, as seen in Fig. 4, were observed, and, on average, the immediate roof consisted of 0.3–1.2 m of silty thinly bedded shales with occasional plant fossils. Above the dark shale were 0.9–1.5 m of lighter-toned, more competent silty shales that lacked the plant fossils of the previous dark shale. Above the light shale was the sandstone 1. Of the approximately 1.5 m of sandstone observed, the bottom of the sandstone was weaker and thinly bedded with mica streaks. However, a few centimeters above the bottom of the sandstone, the mica streaks ceased, and the sandstone became thickly bedded. Generally, the sandstone 1 was lifting up from the first bleeder entry, which was only 23 cm above the Pocahontas Number 3 seam to 1.4 m above the seam in the third bleeder entry.

The visual observations were primarily concerned with changes during the instrumentation period. Although no formal rating scale was used, a qualitative descriptive method was used to document changes in the conditions of the study site. Some of the conditions observed were pot-outs, rib sloughage, horsebacks, slicks, water, and major splits in the coal. Most of the observed conditions were apparent during the initial instrumentation installation during pumpable crib placement. There was minor flaking, enlargement of sloughage, and pot-outs that occurred between the initial observations and the final observations once the face advanced past mid-panel. There was little to no visible floor heave within the instrumented area. However, there was slight floor heave near the gateroads. Although the floor heave was not visible, it was most likely the cause of a substantial portion of the measured convergence. The additional deterioration was associated with local condition changes rather than a pervasive increase in loading of the entire study area.

The instrumentation used in the bleeder study at this mine were load cells (Jackpacks) and convergence monitors (string pots). The Jackpacks are welded metal bags designed for positive loading of standing supports, usually installed on top of cribs [12]. In this application, the fluid pressure in each Jackpack is monitored to record loading of the support. We used both 71-cm-round and 91-cm-square Jackpacks in the sites for the 61 and 91 cm pumpable cribs, respectively. The string pots were either 63 or 38 cm string pots screwed to the upper layer of the pumpable crib, with a wire attached from the string pot to a screw in the lower layer of the pumpable crib. The Jackpacks were installed during the pumpable crib installation. The string pots followed slightly later once the pumpable crib had hardened enough to allow the string pot to be anchored into the pumpable crib. The instrumentation plan is shown in Figs. 5 and 6. Fig. 5 shows the entire instrumentation area that comprises five sites (blue circles). Fig. 6 shows site 1, which is the site located closest to

the gob. Sites 1, 2, and 3 had four instrumented pumpable cribs, each with a Jackpack and a string pot. Sites 4 and 5 each had four instrumented pumpable cribs with a string pot. Sites 1 and 2 had 61-cm pumpable cribs, whereas sites 3, 4, and 5 had 91-cm pumpable cribs. The difference was due to mining height and aspect ratios previously recommended for these types of supports [8]. The locations of the five sites were chosen to provide some difference in applied load due to entry or intersection spans and distance from the longwall gob.

2.3. Results

The resulting convergence of the 20 string pots in the five sites are shown in Fig. 7. Fig. 7 has five vertical lines that represent different positions of the face relative to the startup room. From left to right, the first line is the beginning of the panel, the second line is after 213 m of advance, the third line is after 426 m of advance, the fourth line is 639 m of advance, and the fifth line is approximately mid-panel. In general, the majority of the convergence occurs between the first 213 and 639 m of the panel. There is some convergence before the panel begins, and that is most likely attributed to the shrinking of the pumpable crib while curing. The convergence seen after the first 639 m is relatively minor and likely due to local movement, not related to global loading.

The average convergence experienced by the pumpable cribs at each site is shown in Fig. 8. Fig. 8 depicts the same vertical lines representing the face position. In Fig. 8, almost no movement occurs prior to the panel approaching the 107-m locations. The maximum average convergence at site 3 is less than 1.5 cm. The other four sites show around 1/4–1/2 of a centimeter of convergence. Site 3 shows the most convergence followed by sites 4, 1, 5, and, finally, 2.

The next results are those of the load measured by the Jackpacks underneath the 12 pumpable cribs. Fig. 9 shows the 12 pumpable cribs loading with the same vertical timing lines as Fig. 7. The measured load for the instrumented cribs ranges from 12.7 to 22.7 Mg for the function Jackpacks. The instrumentation on pumpable cribs 5, 20, and 23 were not functioning properly, possible due to leaking. In the case of load, the pumpable cribs in site 1 experience the highest loads while those in sites 2 and 3 are about half as much as site 1.

To lessen the impact of the local effects, the average load for each of the sites is plotted in Fig. 10. Just as for the convergence in Figs. 7 and 8, the load began to increase after about 107 m of face advance. The average load clearly shows that site 1 is taking the most load followed by site 2, and then site 3. It appears that the load has all but stabilized at the end of the measurement period after half of the longwall panel was extracted.

Fig. 11 shows the load versus convergence curve for the three site averages. Both the convergence and the load are relatively small, peaking at about 20 Mg and 1.2 cm of total convergence. The supports at sites 1 and 2 appear to have a similar stiffness—approximately five times that of the supports at site 3.

The results of the visual observations coincided with the instrumented results, and little to no changes were observed throughout the study period. The initial observations were made during the installation of the standing support instrumentation. The initial observations noted

localized areas of slicks and pot-outs, and large fossilized trees that would occasionally fall from the roof. The only major structural feature observed was a lower split of fireclay that occurred in the bottom 61 cm of the main bench that would weaken the lower portion of the ribs. The lower split was only observed on the right side of the last two bleeder entries. Slight additional deterioration was observed in the final visit but was not associated with changing in stress or loading of the rear bleeder entries. The initial and final observations can be seen in Fig. 12.

3. Numerical modeling study

3.1. Model design and methodology

Researchers at NIOSH recently developed a numerical-model-based approach for estimating the changes in both the horizontal and vertical loading conditions induced by an approaching longwall face. In this approach, a systematic procedure is used to estimate the model inputs. Shearing along the bedding planes is modeled with ubiquitous joint elements and interface elements. Coal is modeled with a coal mass model developed at the NIOSH Pittsburgh Mining Research Division (PMRD) [13]. The response of the gob is calibrated with back analysis of subsidence data and the results of previously published laboratory tests on rock fragments. The modeling procedures were verified with the subsidence and stress data recently collected by PMRD from a longwall mine in the eastern United States and with published case studies from both eastern and western U.S. mines [14]. These procedures were followed to create a model of the study site using local rock mass parameters and loading conditions.

The overburden in the study area consists of alternating layers of sandy shale, sandstone, fireclay, and coal. Interfaces between the geological layers in the overburden were modeled with interface elements. Coulomb's criterion was used to define the limiting shear strength of the interfaces. As described by Su, the coefficient of friction of interfaces was set to 0.25 [15,16]. The strongest rock layer was sandstone with a laboratory-scale UCS of approximately 117 MPa. The thickness weighted average of the laboratory-scale UCS of the overburden was approximately 95 MPa.

In developing the Flac3D panel scale model, two initial pseudo-2D models were developed using Flac3D. The first pseudo-2D model was developed employing actual stratigraphy, using all the geological layers from a nearby core hole with a minimum layer thickness of 0.9 m. This model of the mine had 140 different layers with thicknesses ranging from 0.9 to 30.5 m to simulate the overburden. The second pseudo-2D model was developed using a simplified stratigraphy to reduce the number of elements. The lithology and mechanical properties of the second model were based on thickness averaging to reduce the total number of layers and elements in the model. The second model had element sizes, lithology, and mechanical properties identical to the final 3D model used to evaluate the mining conditions and stresses. Once both pseudo-2D models were developed, the stresses were compared (see Fig. 13), and they were found to be similar enough to use the second pseudo-2D model overburden geometry and properties in the full 3D model. Vertical stress on the coal pillars and subsidence calculated from the first pseudo-2D model were comparable to the previous experience at the mine [16].

Due to the large size of the modeled area, it was impractical to use element sizes as small as 0.9 m in the 3D model. Therefore, equivalent elements based on the thickness weighted mechanical properties were used to simulate the combination of layers less than 9 m in thickness. In order to simulate the sliding and separation of the thin layers accurately, an elastic transversely isotropic material model was used to simulate equivalent layers. The stability mapping grid generator is used to generate the mine layout at the seam level [17]. The instrumented bleeder entries, pillars, roof, and floor were simulated with 0.9-m elements in the detailed area (Fig. 14). The methodology defined by Tulu, Esterhuizen, Mohamed, and Klemetti was used to derive in situ material properties for the detailed area (Table 1) [14]. The coal material properties published by Mohamed, Tulu, and Murphy were used to simulate the coal material [13]. The rest of the seam level elements in the model were 4.6 m in thickness. The geometry of the model can be seen in Fig. 15. The representative geological sequence that was modeled is shown in Fig. 16.

3.2. Results

The numerical modeling results can be separated into three categories: (1) the overall stress redistribution pattern for the entire area due to development and abutment loading, (2) the three cross sections shown in Fig. 2, and (3) the area of interest in the bleeder entries behind longwall panel 2. All three categories calculated stress and displacements of each model element. The overall stress redistribution (category 1) appears as expected in terms of stress increases and decreases with the various states of mining. The cross sections (category 2) are shown in Fig. 2—*AA, BB,* and *CC*. Cross section *AA* runs the length of longwall panel 2 from the bleeders to about 610 m outby. Cross section *BB* runs across the two panels and the barrier pillar about 366 m outby the startup room. This cross section was included to compare to the pseudo2D models and past measured results of gateroad loading and convergence. Cross section *CC* runs through the four rear bleeder pillars, parallel to the panel length, from the furthest entry from the gob to the first entry after the barrier pillar. Category 3, bleeder entries, shows that loads increase closer to the gob and closer to an intersection, as expected.

The overall stress distribution due to the development of the entries, extraction of longwall panel 1, and extraction of longwall panel 2 can be seen in Fig. 17. The development of the gateroads and bleeder entries shows an increase in stress very close to the opening mined. During the extraction of the first panel, Fig. 17 shows a reduction of stress in the gob and an increase in stress in the gateroads and bleeders, all as expected. The final stage, or once extraction of the second panel is complete, shows additional stresses added to the gateroads of panel 1, as well as panel 2, and more evenly distributed stresses in the gob by way of increasing stress in lower-stress areas (Fig. 15).

Figs. 18 and 19 show the results of the vertical stress on cross section *AA*. Fig. 18 is a colored plot of the final stress across the modeled area. The middle gateroad pillars experience the greatest load. Fig. 19 is a chart showing the numerical stresses in cross section *AA*. The gob load is approaching half the in situ stress, and the pillar behind the startup room is seeing significant loading due to the extraction of the longwall panel. The bleeder entries show minor increases in load overall at the final modeling stage; however,

there appears to be a slight decrease in pillar load the farther away from the gob the pillar is located.

The cross section *BB* perpendicular to the mining direction focuses on the loading of the gateroads during mining. Fig. 20 is a colored plot of the final results of the model after mining the longwall panel 2. The results are as expected, with the middle gateroad showing the highest stress and the first gob having slightly higher stress. Fig. 21 is a chart of the numerical values along cross section *BB*. The gob stresses after mining are approximately half the in situ stress, and the side abutment stresses peak at around 83 MPa, with both as expected for a subcritical panel surrounded by strong strata. The furthest left gateroad also experienced slightly greater stress than the gateroad furthest to the right.

The final result concerning the cross section is that of the cross section *CC* through the bleeder pillars parallel to the panel length. The colored plot in Fig. 22 depicts the final stresses in the bleeder pillars. There is a slight increase in stress in the pillar closest to the gob with the pillar farthest from the gob having the lowest stress of the bleeder pillars. Fig. 23 shows the progression of stresses along the cross section *CC* from in situ through the extraction of the second longwall panel. After development mining, there are only slight increases in the stress due to the subsequent longwall extraction.

Fig. 24 expands on Fig. 23, demonstrating and providing quantitative values for the average bleeder pillar stress at the three phases of the numerical model: development, first panel, and second panel. In comparison to the in situ stress, the development state provides the greatest change in pillar stress. The mining of the second panel only slightly increases the pillar stresses by about 0.7–1.4 MPa.

The final modeling results are associated with the convergence in the area of interest. The convergence was calculated by combining the roof sag and the floor heave. The convergence, much the same as stresses, tends to decrease while moving further away from the gob, assuming all other conditions are the same. The convergence is also slightly greater in four-way intersections compared to three-way intersections, which both show slightly greater convergence than in entry straights. Overall, in this model, the convergence is very minimal; less than 0.8 cm of convergence was modeled between the first and second panel.

3.3. Discussion

The focus of this study is primarily on the redistribution of stress in the bleeder entries due to longwall mining. The instrumentation provides insight into the state of the standing support and confirmed our expectation of load in the rear bleeders being greater approaching the gob or approaching intersections, with the former being of greater influence. The numerical modeling provides insight into the timing of the load transfer and the magnitudes of the load transfer to the pillars, gob, solid coal, and support elements.

Some of the more intriguing results of this study are the in situ load displacement curves of the pumpable cribs versus the laboratory testing results of the pumpable cribs, as seen in Fig. 25. The supports installed in the study site show less than 20% of the yield strength and an even lesser percentage of convergence that the supports are capable of withstanding while

still providing support. A maximum of 22.7 Mg was measured on the instrumented pumpable cribs, and their yield load is rated between 159 and 226 Mg. Likewise, the maximum measured convergence is 2.3 cm (likely an anomalous reading)—about half the yield convergence of 5.1 cm. The more typical convergence measured is around 0.64 cm, or less than 1/8th the yield convergence of the pumpable cribs installed.

Another promising result is the ability of the numerical modeling procedure to capture reasonably well the convergence measured in the standing support. Fig. 26 shows that the average measured convergence at all five sites is near the modeled convergence. The numerical model shows that between 0.26 and 0.51 cm of convergence is well within the range of measured results, excluding the outlier of 2.3 cm.

4. Conclusions

In this particular installation, the load and convergence of the instrumented pumpable cribs was significantly less than their capacities. The measured convergence was less than the critical 5.1–10.2 cm that indicates the need for the pumpable cribs. Even the outlier 2.3 cm of measured convergence is less than the typical value of Australian TARP level Red [18]. Finally, the numerical models used in this study effectively represent the instrumentation results, visual observations, and expected outcomes of the mining modeled. The calibrated model shows that, after development mining, there are only slight increases in the stress due to the subsequent longwall extraction. In very similar conditions, the model could be used to evaluate alternative mine designs, possibly including pillar, intrinsic supports, and standing supports to enhance safety of mine personnel.

References

[1]. Peng SS. Longwall mining. 2nd ed. Morgantown, WV: West Virginia University, Department of Mining Engineering; 2006 p. 621.

[2]. Hill D, Stone R, Suchowerska A, Trueman R. Pillar abutment loading–new concepts for coal mining industry. In: Proceedings of the 15th coal operators' conference New South Wales, Australia: University of Wollongong; 2015 p. 204–11.

[3]. Mark C. Analysis of longwall pillar stability (ALPS): an update; Proceedings of the workshop on coal pillar mechanics and design; U.S. Department of the Interior, Bureau of Mines. 1992. 239–49. Information Circular 9315

[4]. Mark C, Chase FE. Analysis of retreat mining pillar stability (ARMPS). In: Proceedings of new technology for ground control in retreat mining U.S. Department of Health and Human Services, Centers for Disease Control and Prevention, National Institute for Occupational Safety and Health Information Circular 94446; 1997 p. 17–34.

[5]. Mishra B, Tang X. Stability analyses of bleeder pillars in longwall mines by displacement-discontinuity method. Int J Min Sci Technol 2015;25(6):933–41.

[6]. Zhang P, Milam M, Mishra M, Hudak WJ, Kimutis R. Requirements and performance of pumpable cribs in longwall tailgate entries and bleeders. In: Peng SS, editor. Proceedings of the 31st international conference on ground control in mining Morgantown, West Virginia: West Virginia, West Virginia: West Virginia University; 2012 pp. 1–11.

[7]. Barczak TM, Tadolini S, Zhang P. Evaluation of support and ground response as longwall face advances into and widens pre-driven recovery room. In: Peng SS, editor. Proceedings of the 26th international conference on ground control in mining Morgantown, WV: West Virginia University; 2007 p. 160–72.

[8]. Campoli AA. Selection of pumpable cribs for longwall gate and bleeders entries. In: Barczak TM, editor. Proceedings of the 34th international conference on ground control in mining Morgantown, WV: West Virginia University; 2015 p. 80–2.

[9]. Batchler T. Peng SS. Analysis of the design and performance characteristics of pumpable roof supports; Proceedings of the 35th international conference on ground control in mining; Morgantown, WV: West Virginia University. 2016. 169–78.

[10]. Barczak TM. Optimizing secondary roof support with the NIOSH Support Technology Optimization Program (STOP). In: Peng SS, editor. Proceedings of the 19th international conference on ground control in mining Morgantown, WV: West Virginia University; 2000 p. 74–83.

[11]. Barczak TM. Updating the NIOSH Support Technology Optimization Program (STOP) with new support technologies and additional design features. In: Peng SS, editor. Proceedings of the 20th international conference on ground control in mining Morgantown, WV: West Virginia University; 2001 p. 337–46.

[12]. Heintzmann. Jack Pot: pre-stressing device. Heintzmann Corp; 2017 <http://www.heintzmann.eu/index.php?id=prestressing_devices>.

[13]. Mohamed KM, Tulu IB, Murphy MM. Numerical model calibration for simulating coal ribs. In: Proceedings of the 35th international conference on ground control in mining Morgantown, WV: West Virginia University; 2016 p. 10.

[14]. Tulu IB, Esterhuizen GS, Mohamed K, Klemetti TM. Verification of a calibrated longwall model with field measurements In: Unpublished paper for upcoming: 51st US Rock Mechanics/Geomechanics Symposium. San Francisco, CA: American Rock Mechanics Association; 2017.

[15]. Su DWH. Finite element modeling of subsidence induced by underground coal mining: the influence of material nonlinearity and shearing along existing planes of weakness. In: Peng SS, editor. Proceedings of the 10th international conference on ground control in mining Morgantown, WV: West Virginia University; 1991 p. 287–300.

[16]. Su DWH. Personal communication; 2016.

[17]. Wang Q, Heasley KA. Stability mapping system. In: Peng SS, editor. Proceedings of the 24th international conference on ground control in mining Morgantown, West Virginia: West Virginia University; 2005 p. 243–9.

[18]. NSW. Strata control in underground coal mines. NSW Code of Practice: WHS (Mines) Legislation. Trade & Investment Mine Safety. State of New South Wales through the Department of Trade and Investment; 2017 <http://www.resourcesandenergy.nsw.gov.au/__data/assets/pdf_file/0003/543945/NSWcode-of-practice-Strata-control-in-undergound-coal-mines.pdf>.

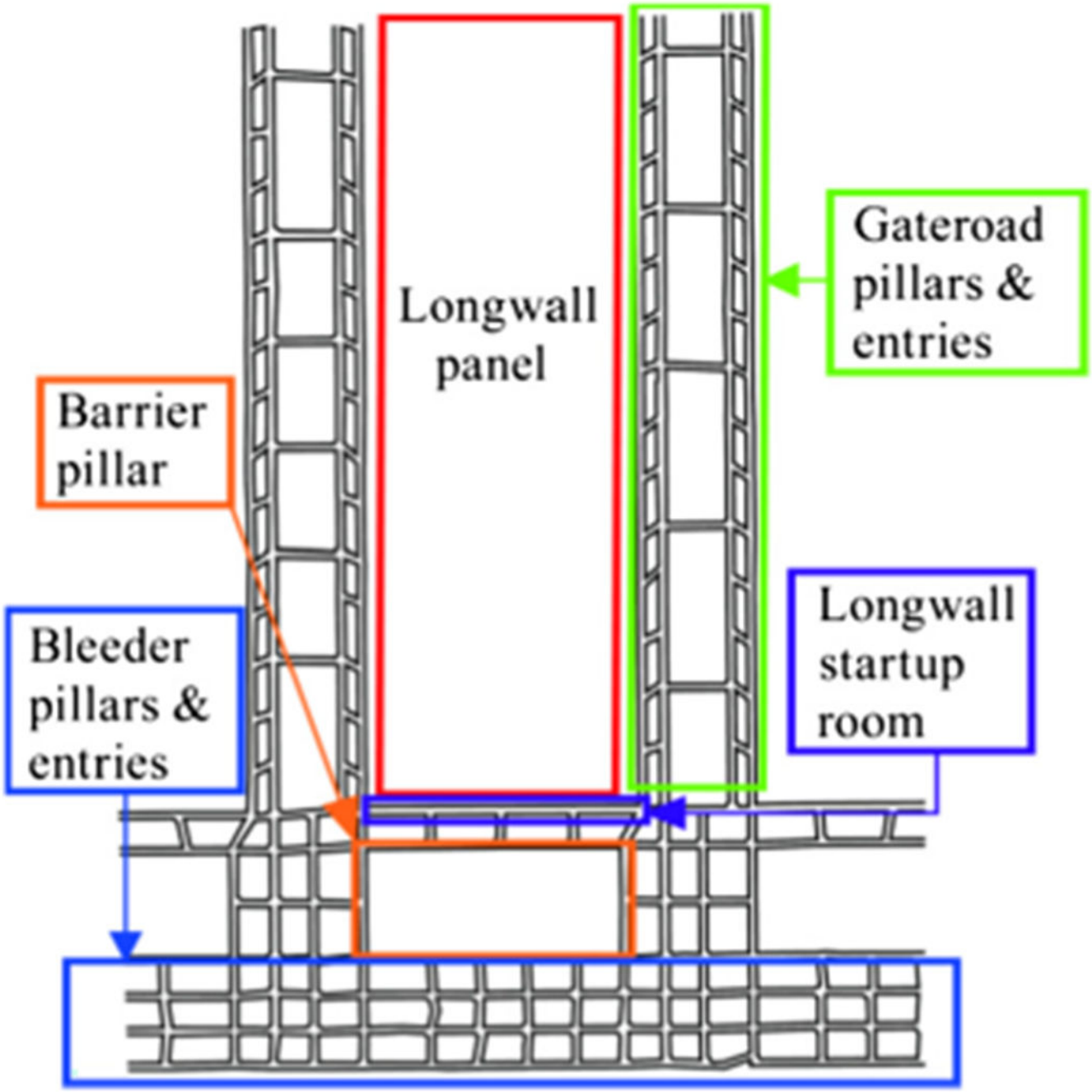

Fig. 1.
A generalized layout of a longwall mine.

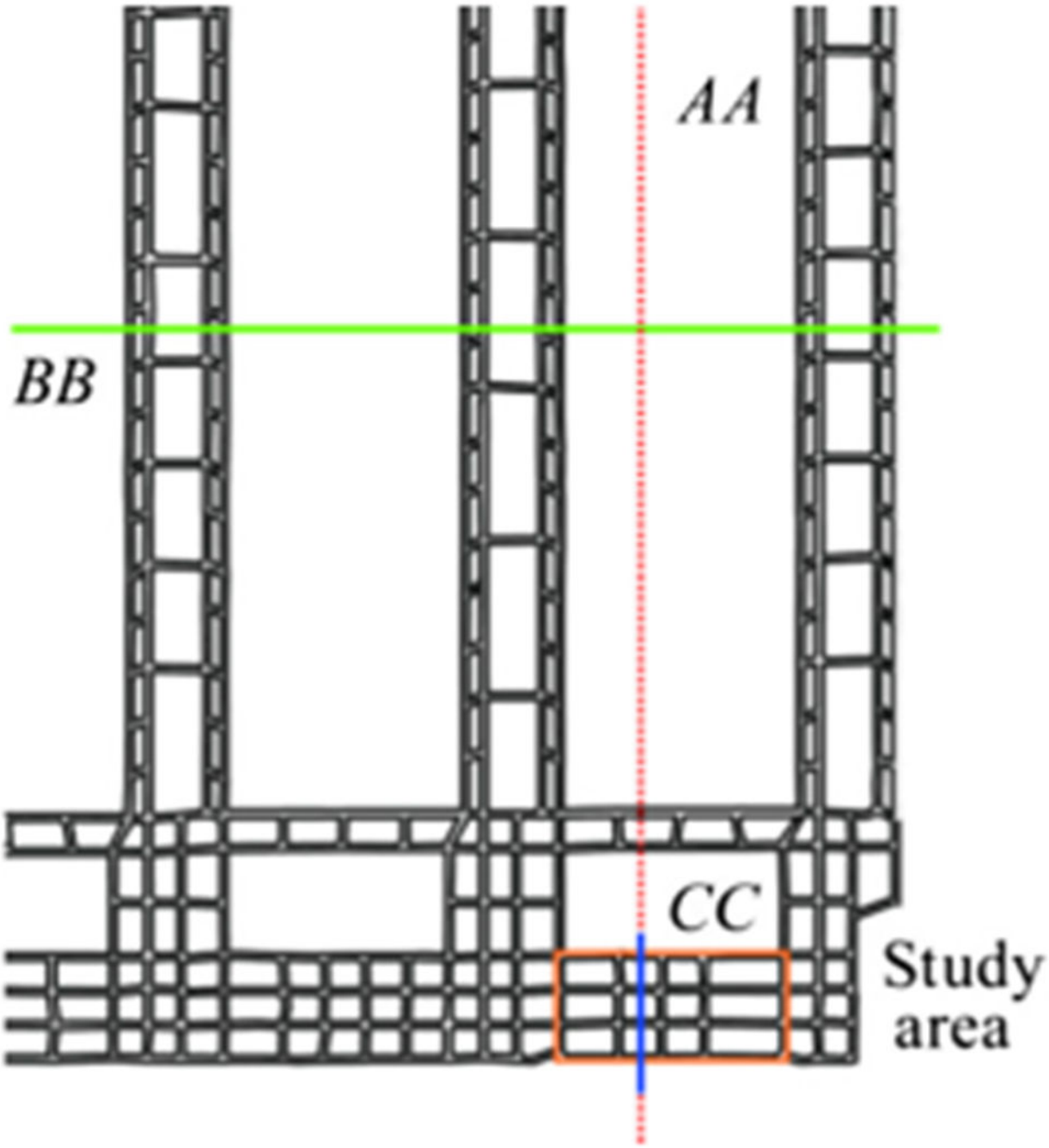

Fig. 2.
A layout of the study mine showing the cross sections and study area.

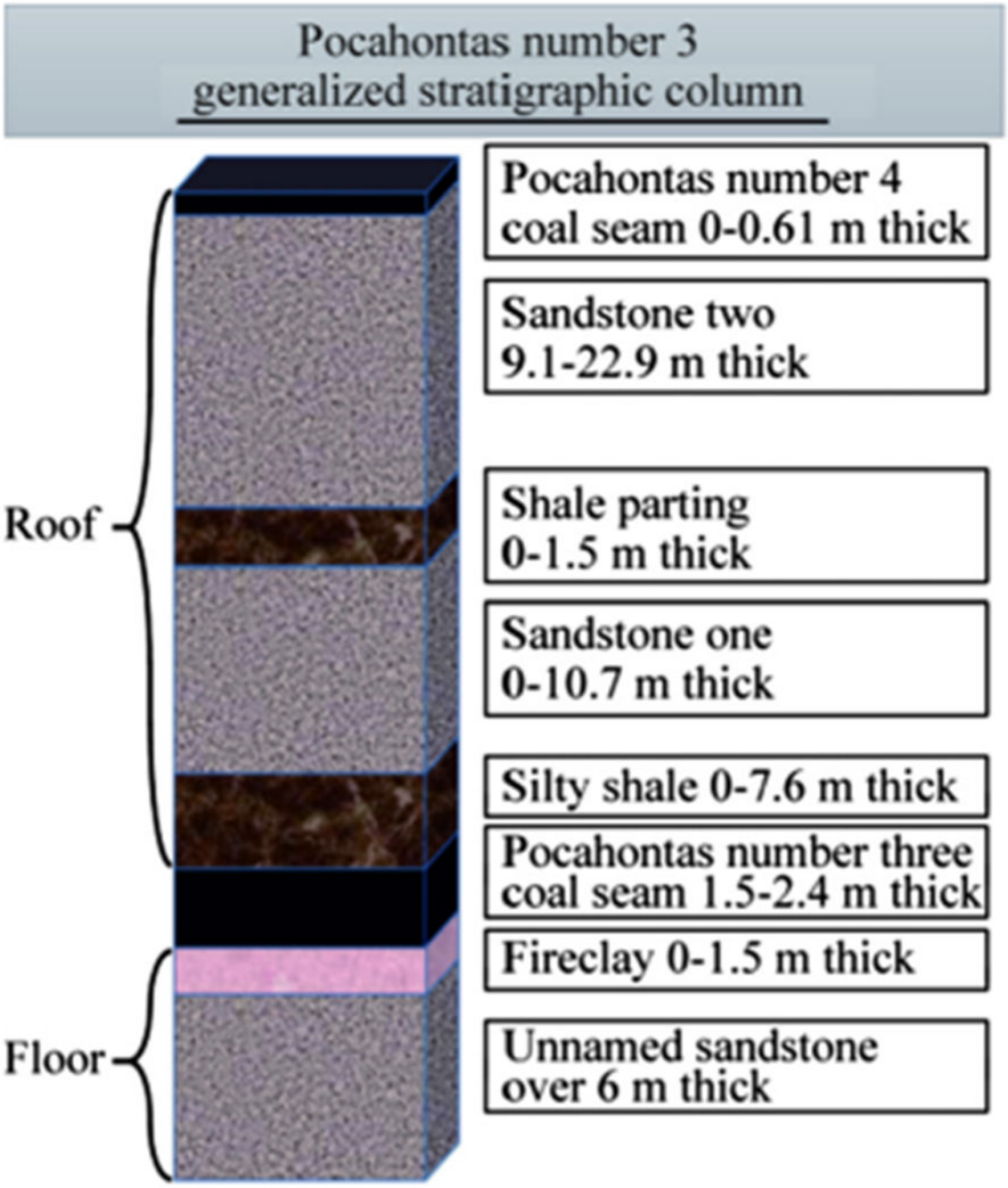

Fig. 3.
A generalized stratigraphic column of the Pocahontas Number 3.

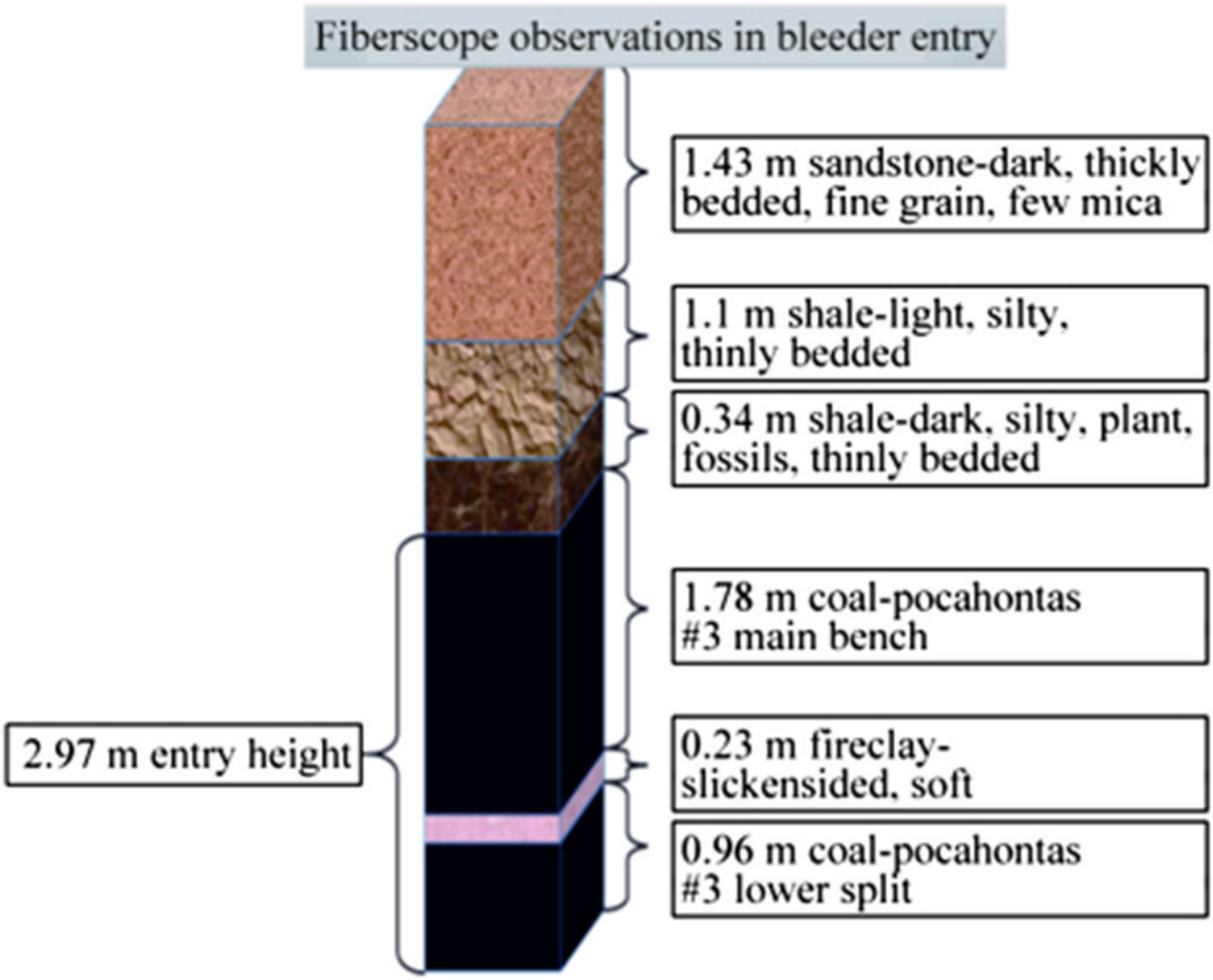

Fig. 4.
A stratigraphic column of the third bleeder entry in the study site.

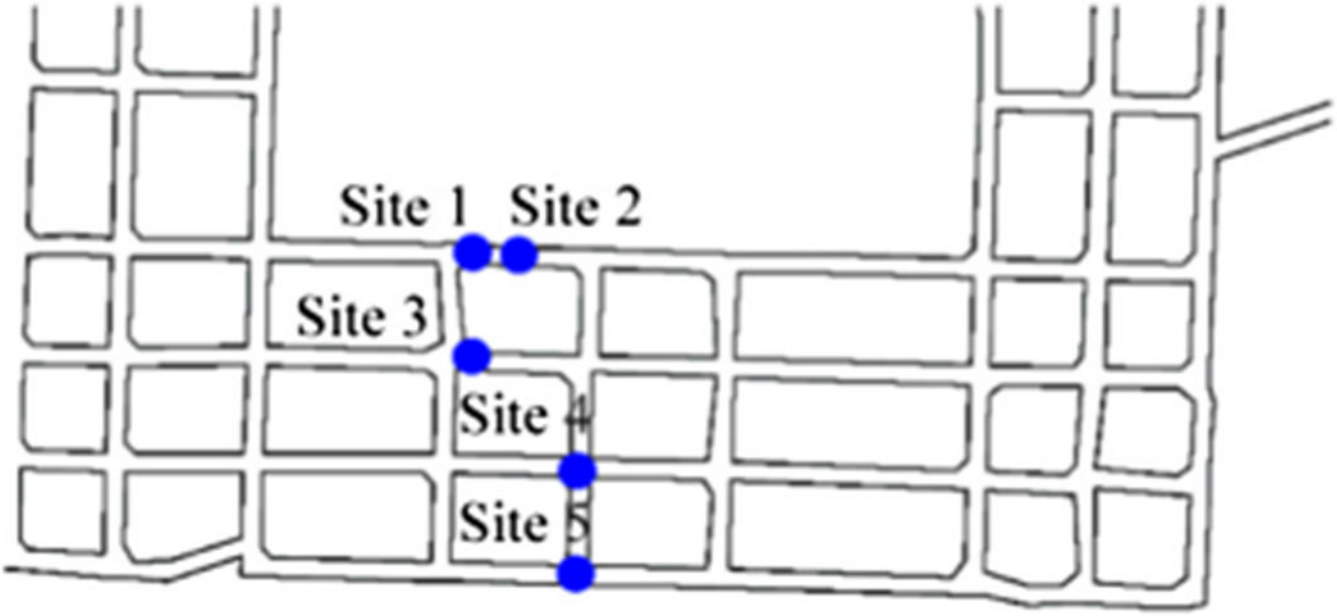

Fig. 5.
Overall layout of the instrumented pumpable cribs and the observational area.

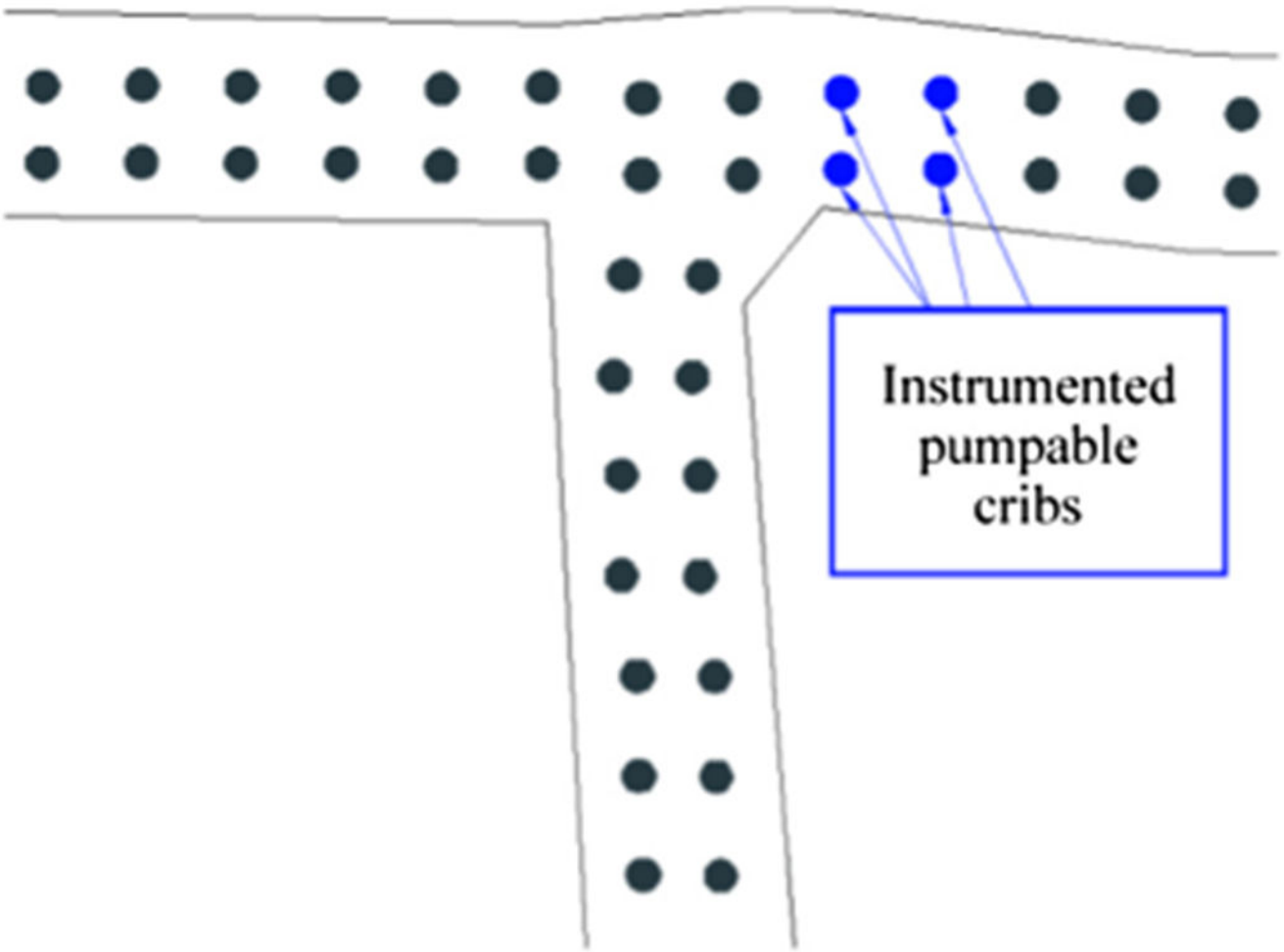

Fig. 6.
Layout of site 1 instrumented pumpable cribs.

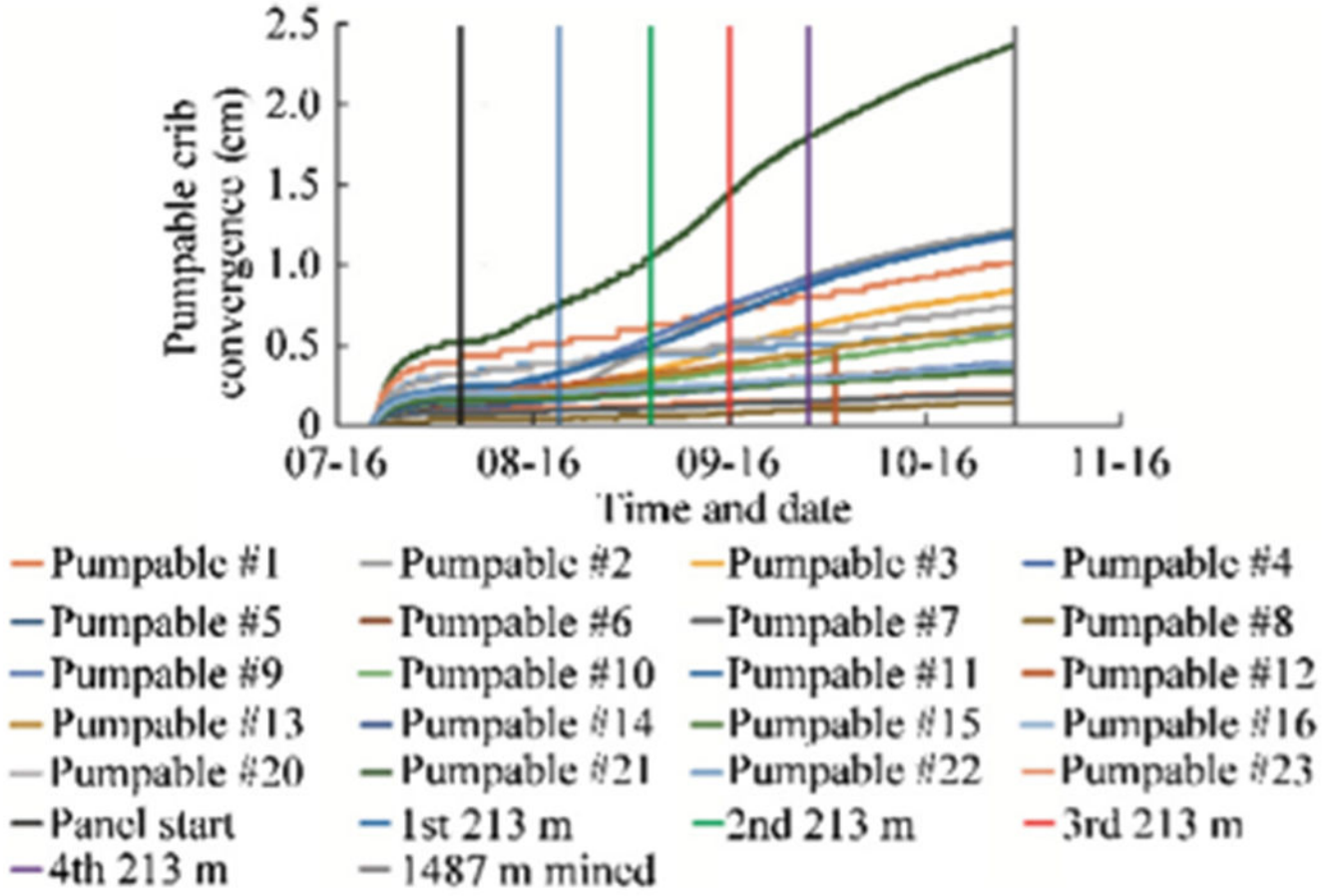

Fig. 7.
Measured convergence of the pumpable cribs in the study area.

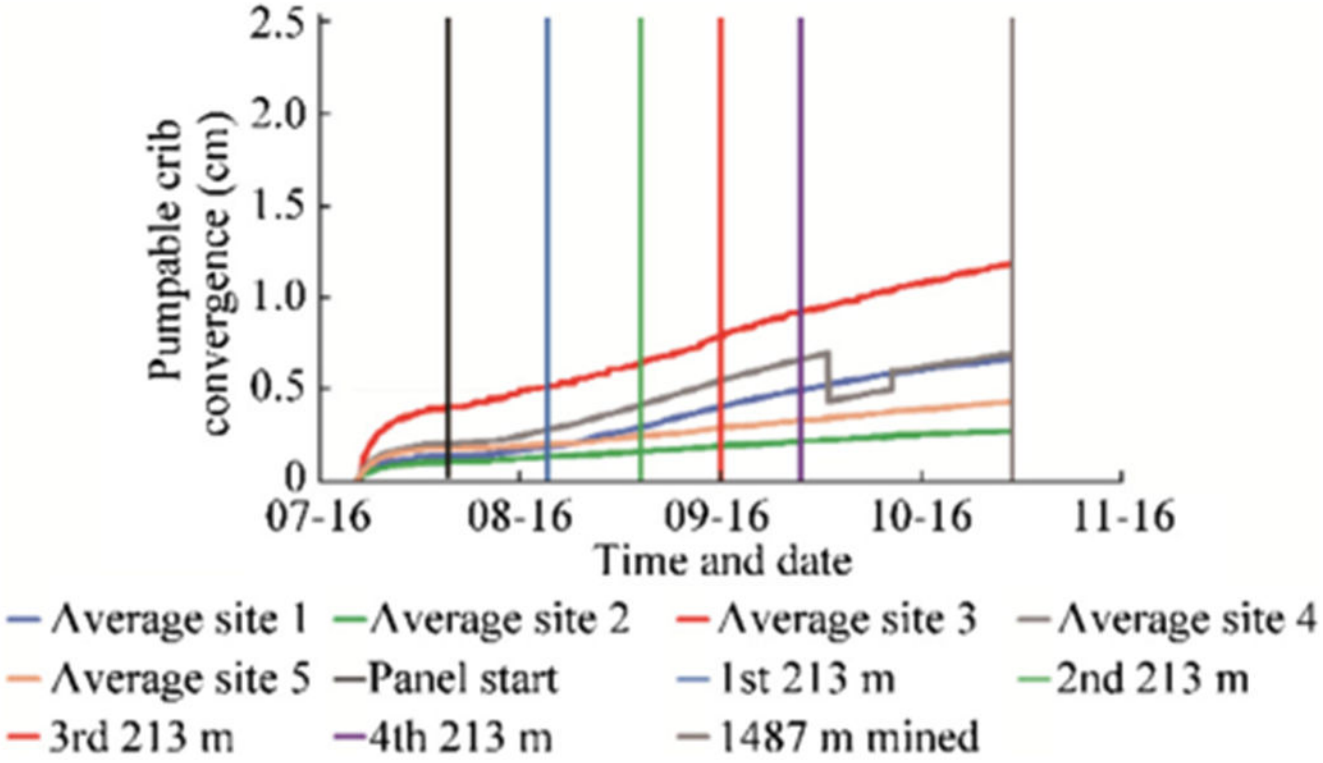

Fig. 8.
Average measured convergence of the pumpable cribs for each of the five sites.

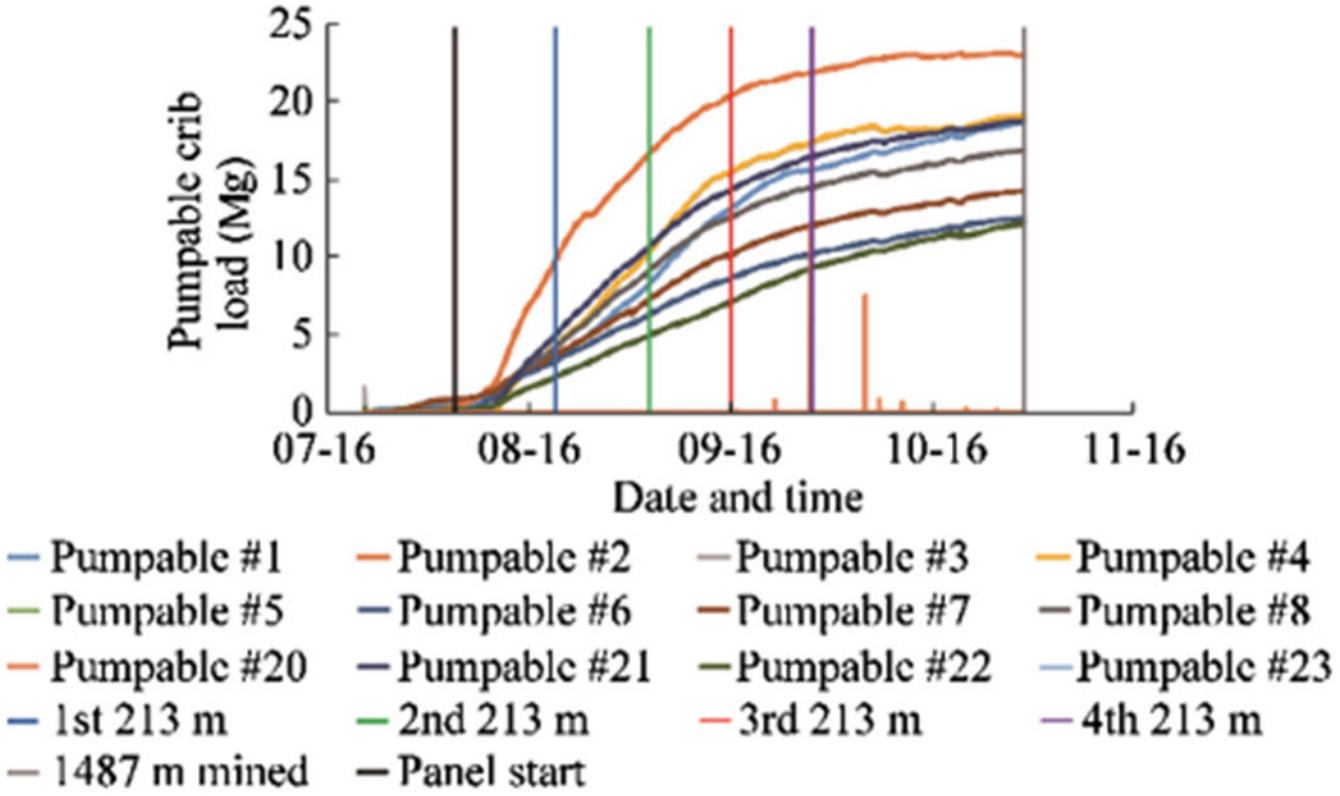

Fig. 9.
Measured load of the pumpable cribs in the study area.

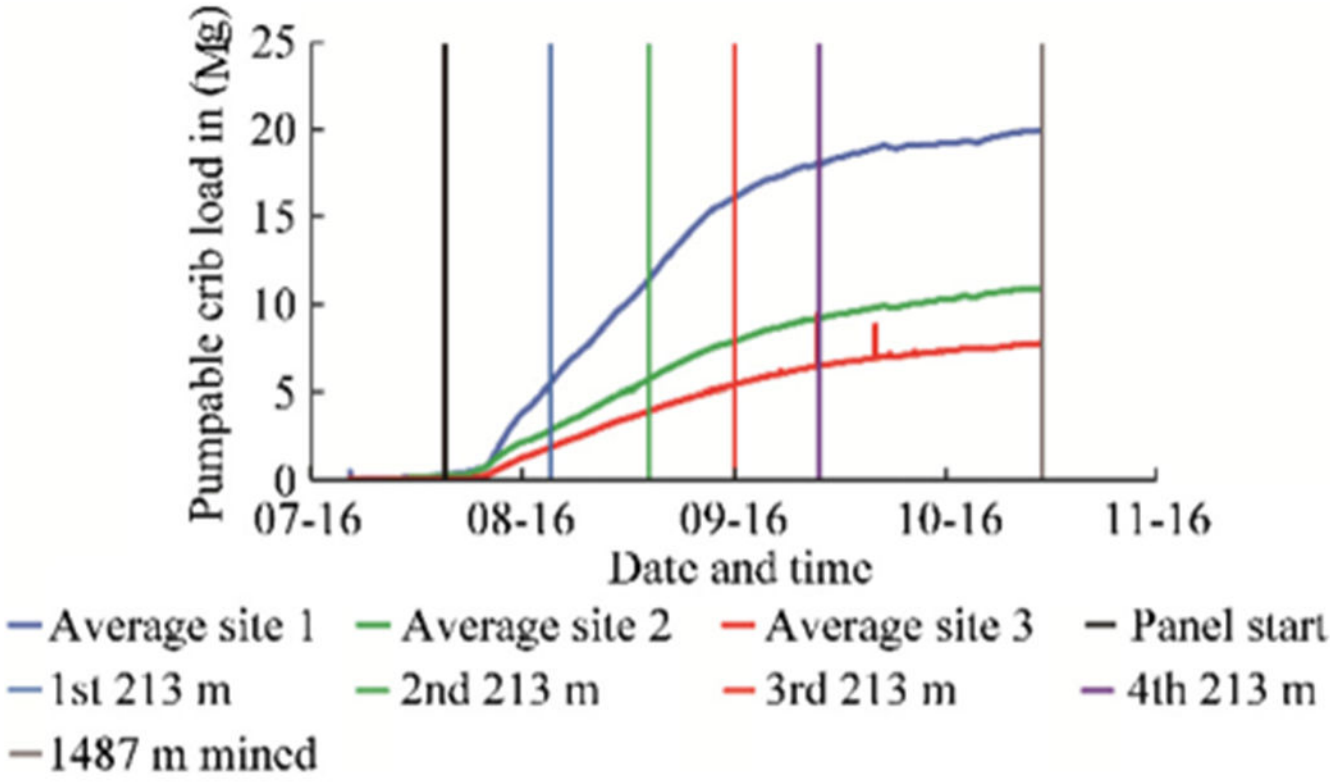

Fig. 10.
Average measured load of the pumpable cribs for each of the three sites.

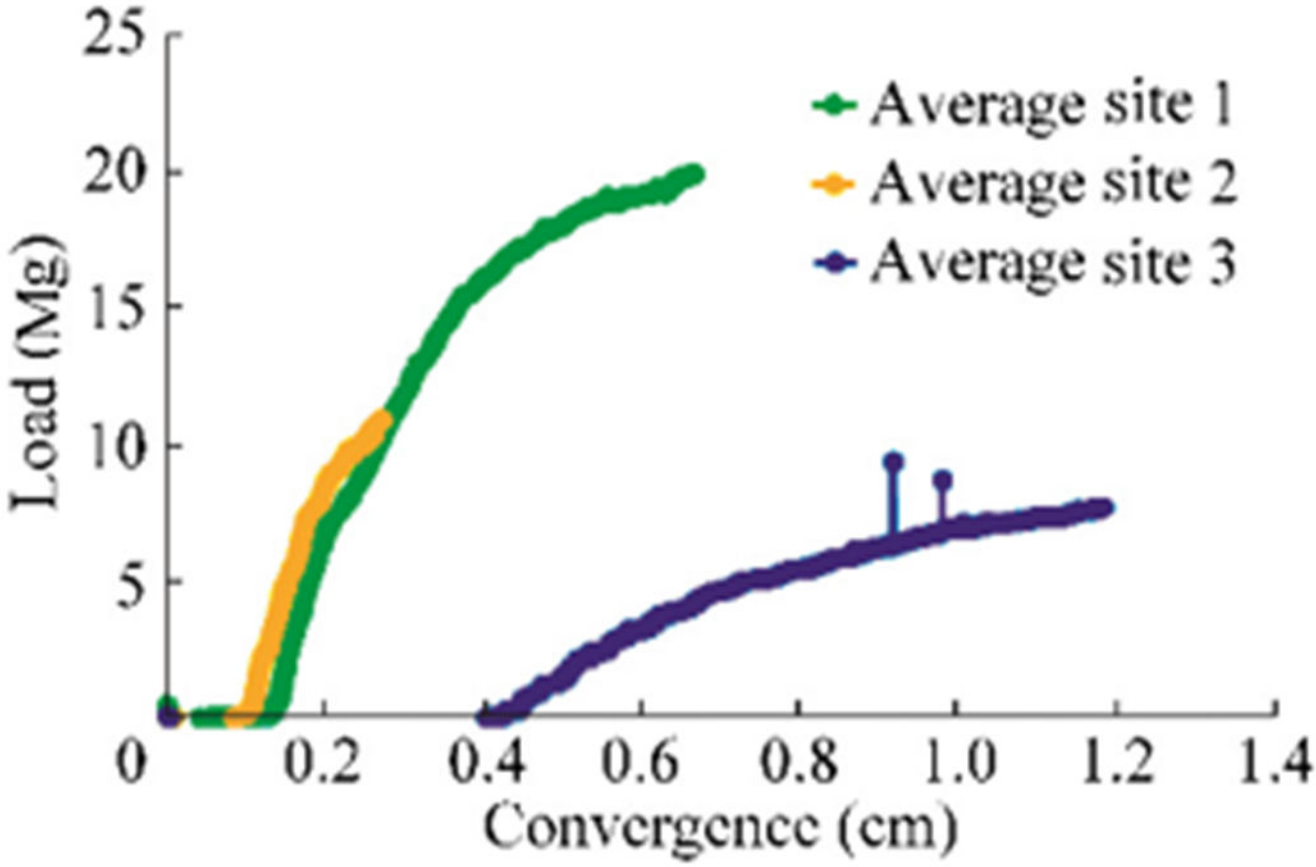

Fig. 11.
Average measured performance curves for the pumpable cribs in each of the three sites, load vs displacement.

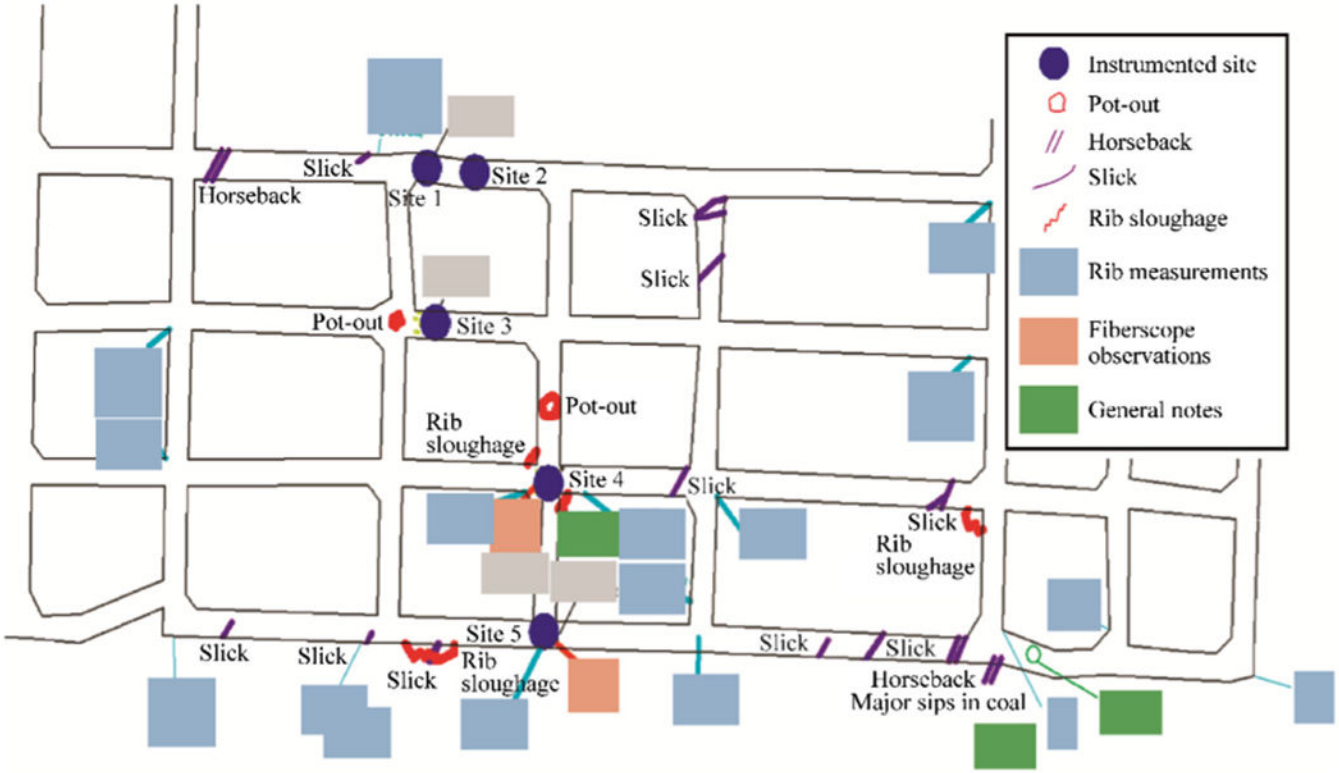

Fig. 12.

The visual observations of the study area throughout the entire study period.

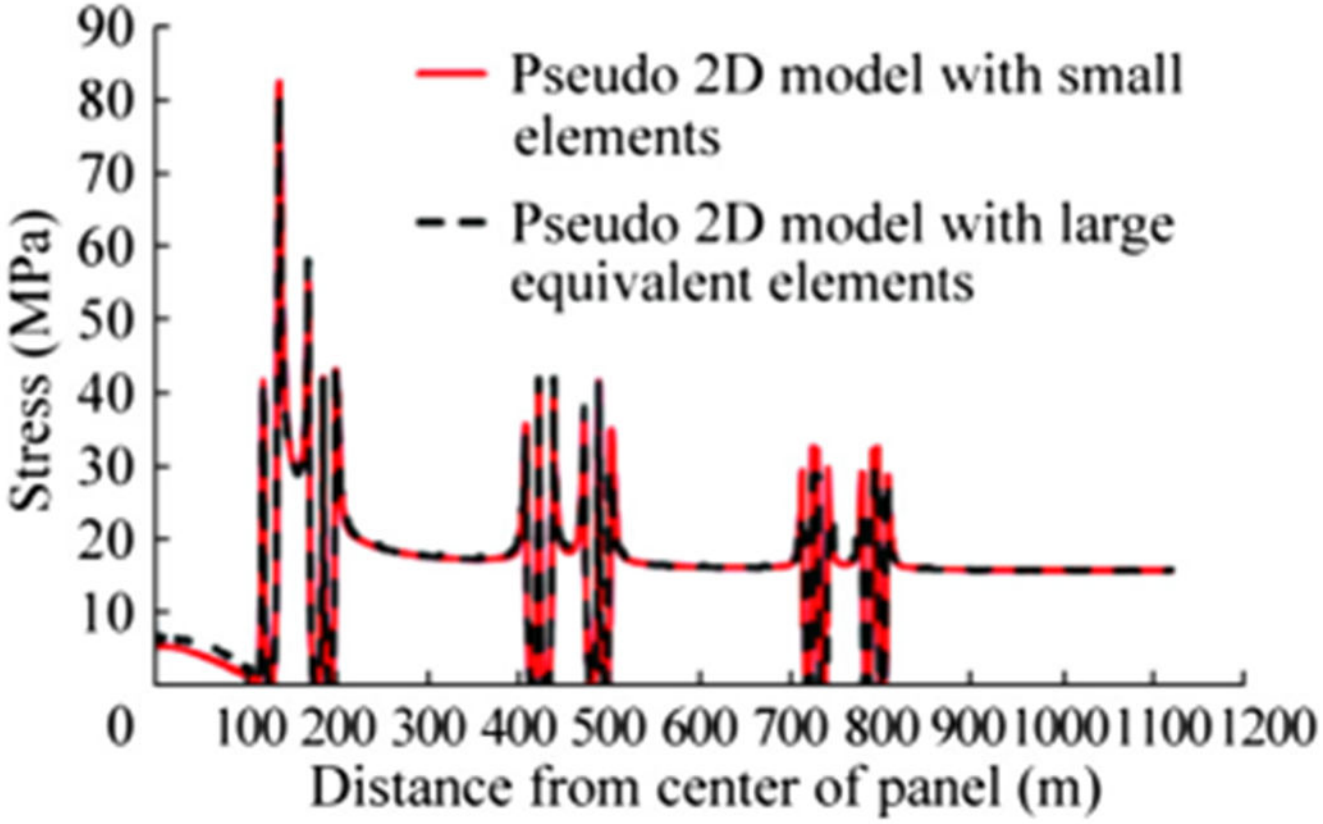

Fig. 13.
Comparison of the stresses calculated by the two pseudo 2D Flac3D models.

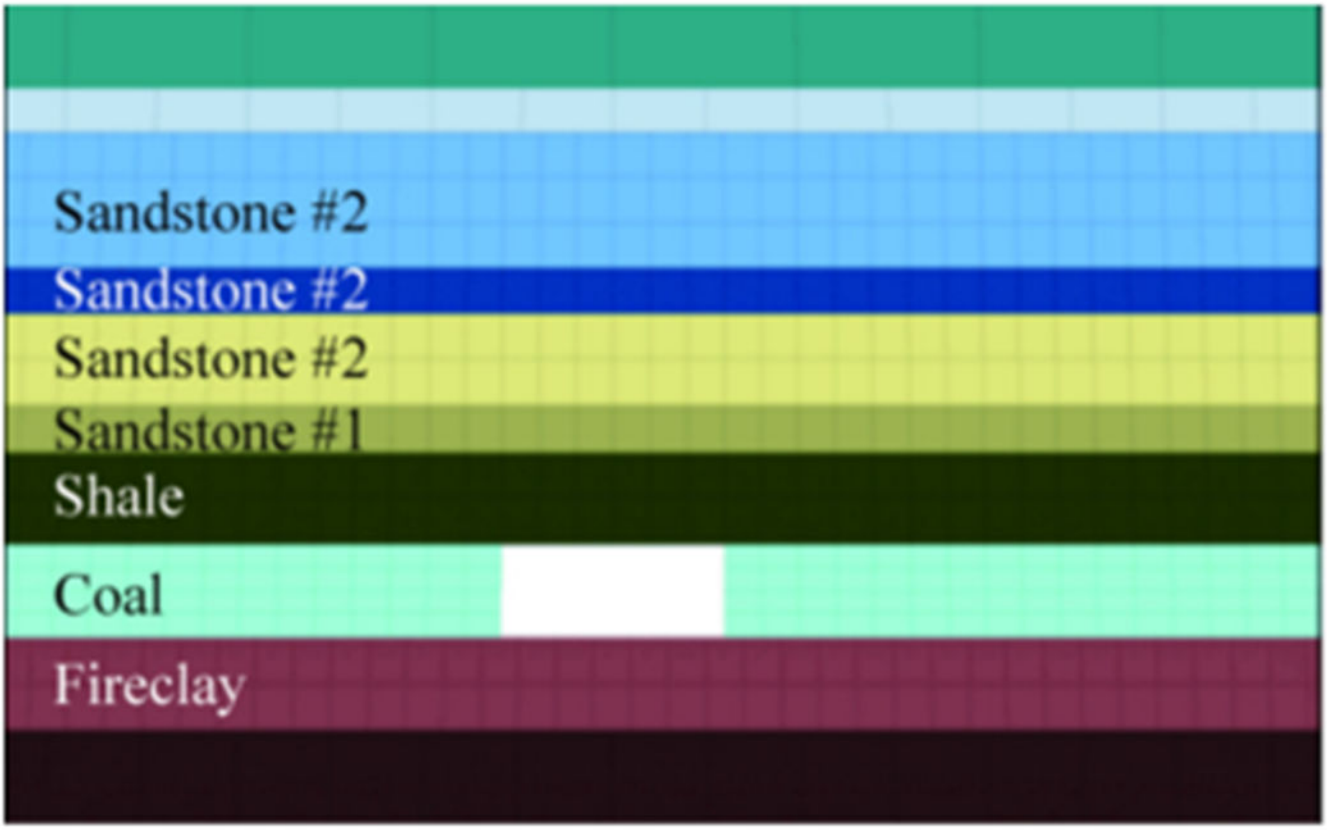

Fig. 14.
Depiction of the entry, coal, and immediate roof and floor material for final 3D model.

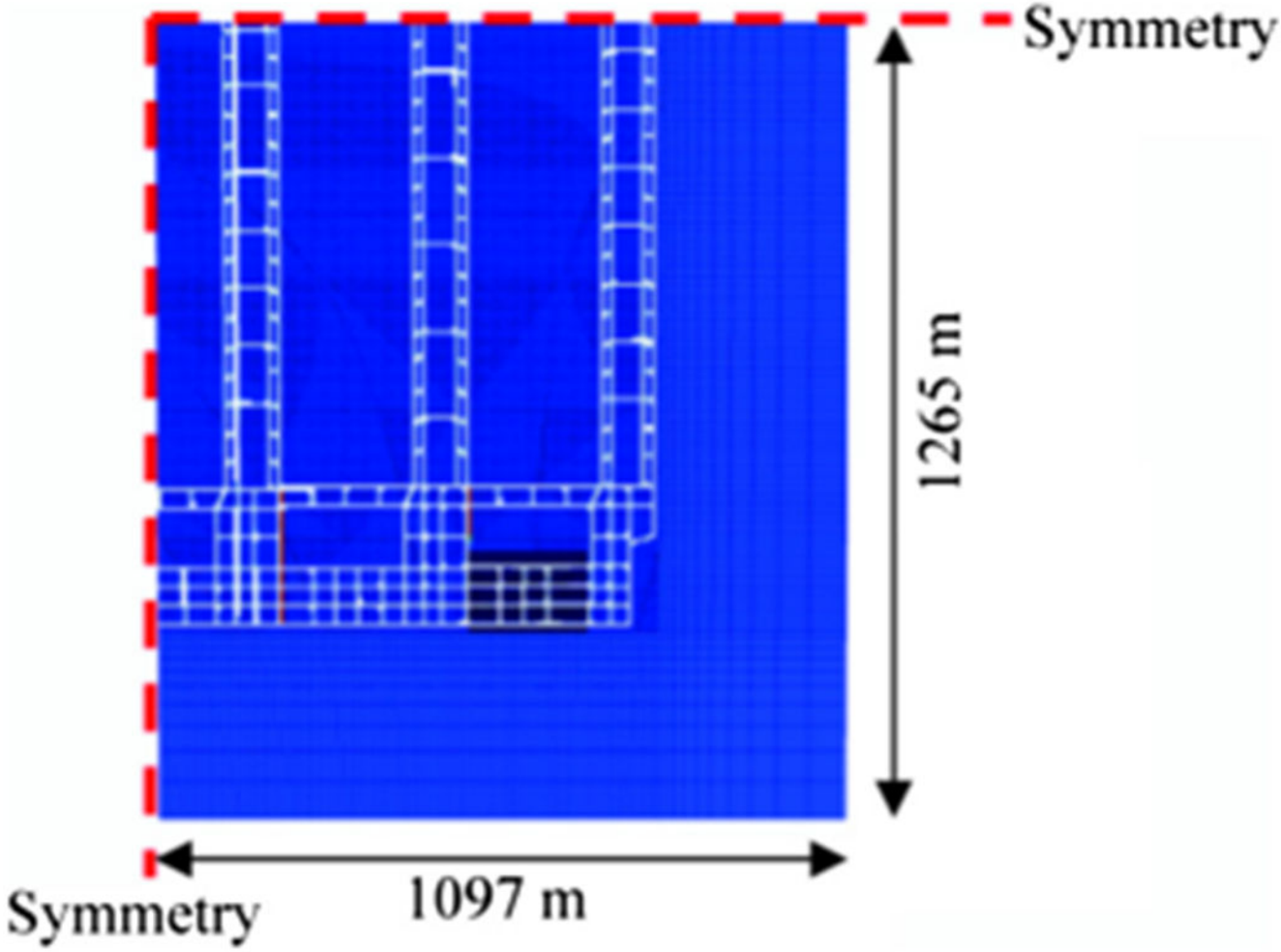

Fig. 15.
Geometrical layout of the 3D model.

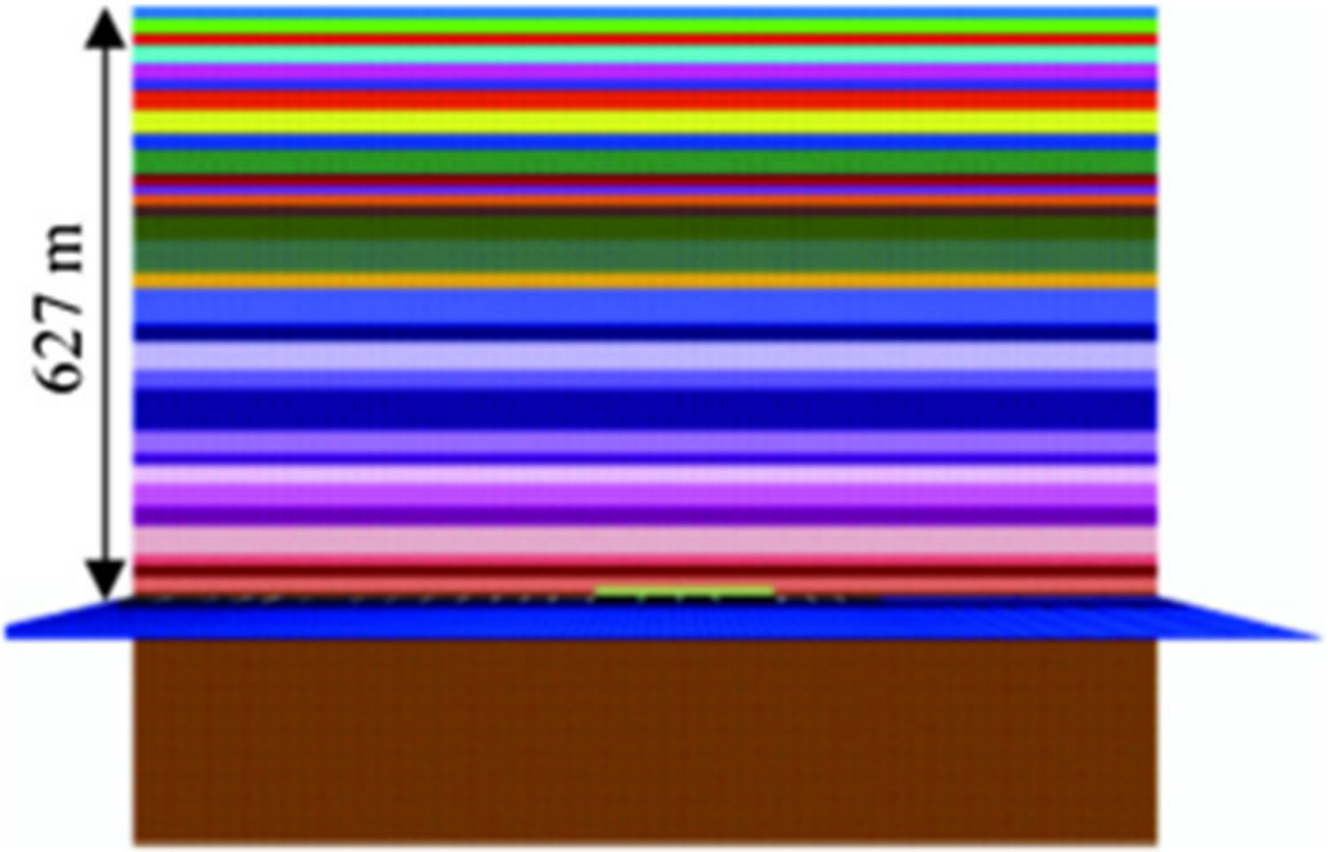

Fig. 16.
Depiction of the overburden of the entire 3D model used to evaluate the bleeders.

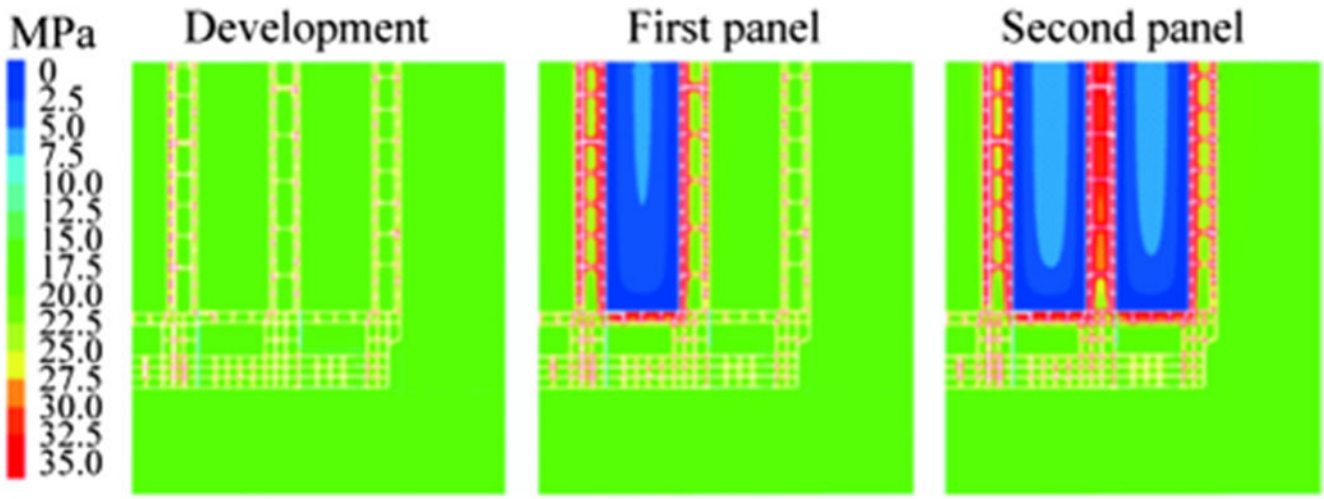

Fig. 17.
Progression of stress through the mining within the study site.

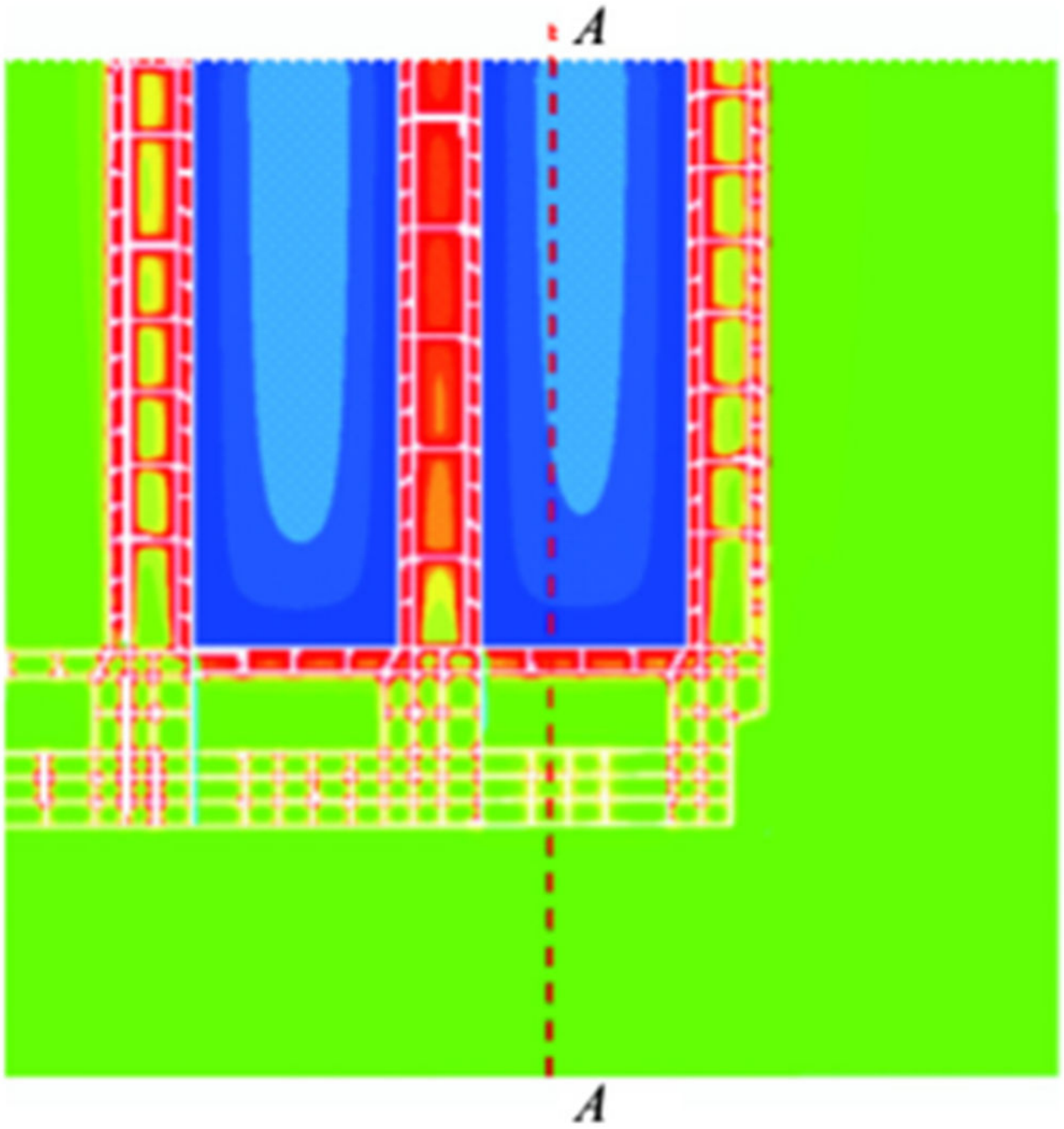

Fig. 18.
Colored plot of the stress in the model due to the extraction of the two longwall panels.

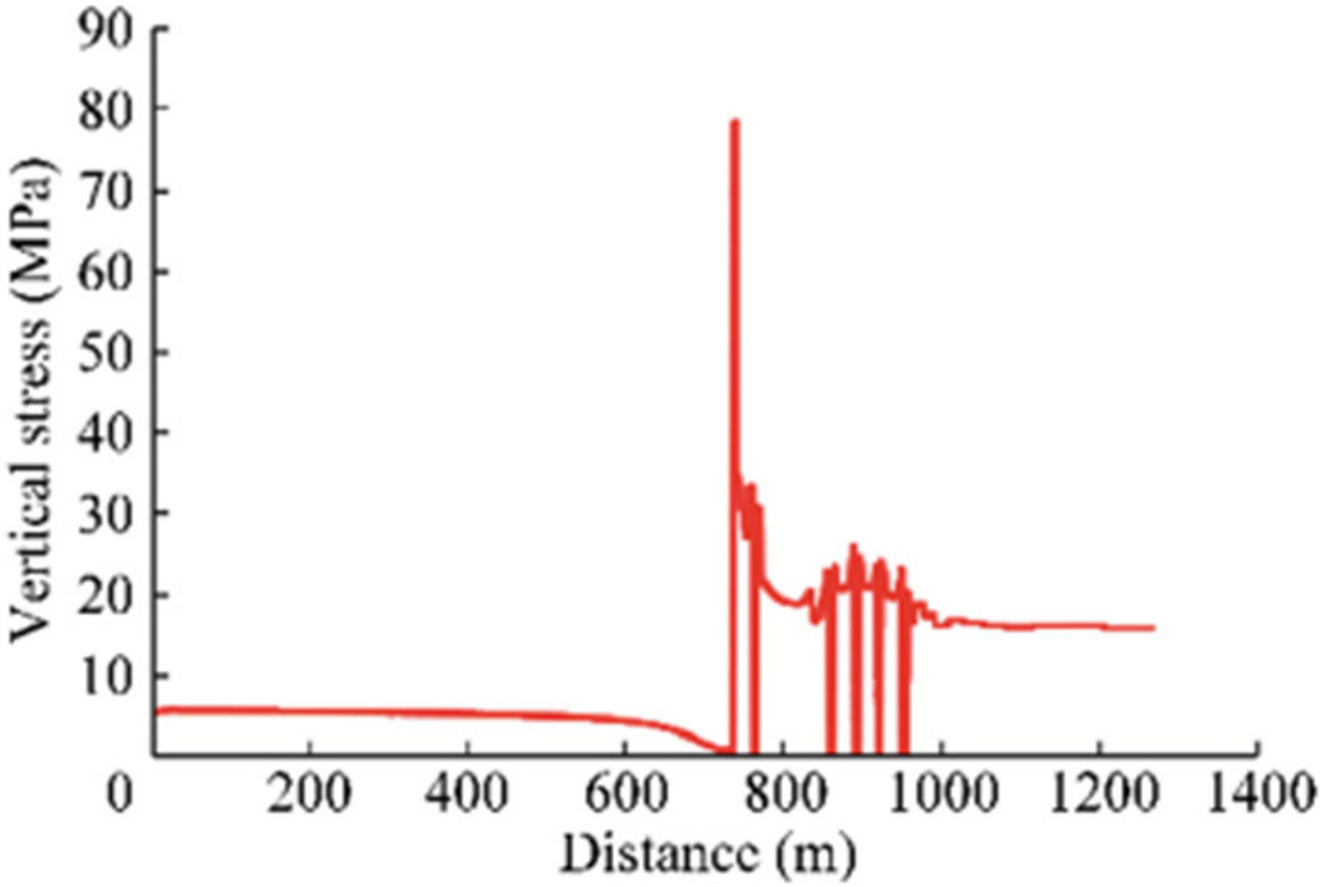

Fig. 19.
Chart of the stress along cross section *AA* once the longwall panel was extracted.

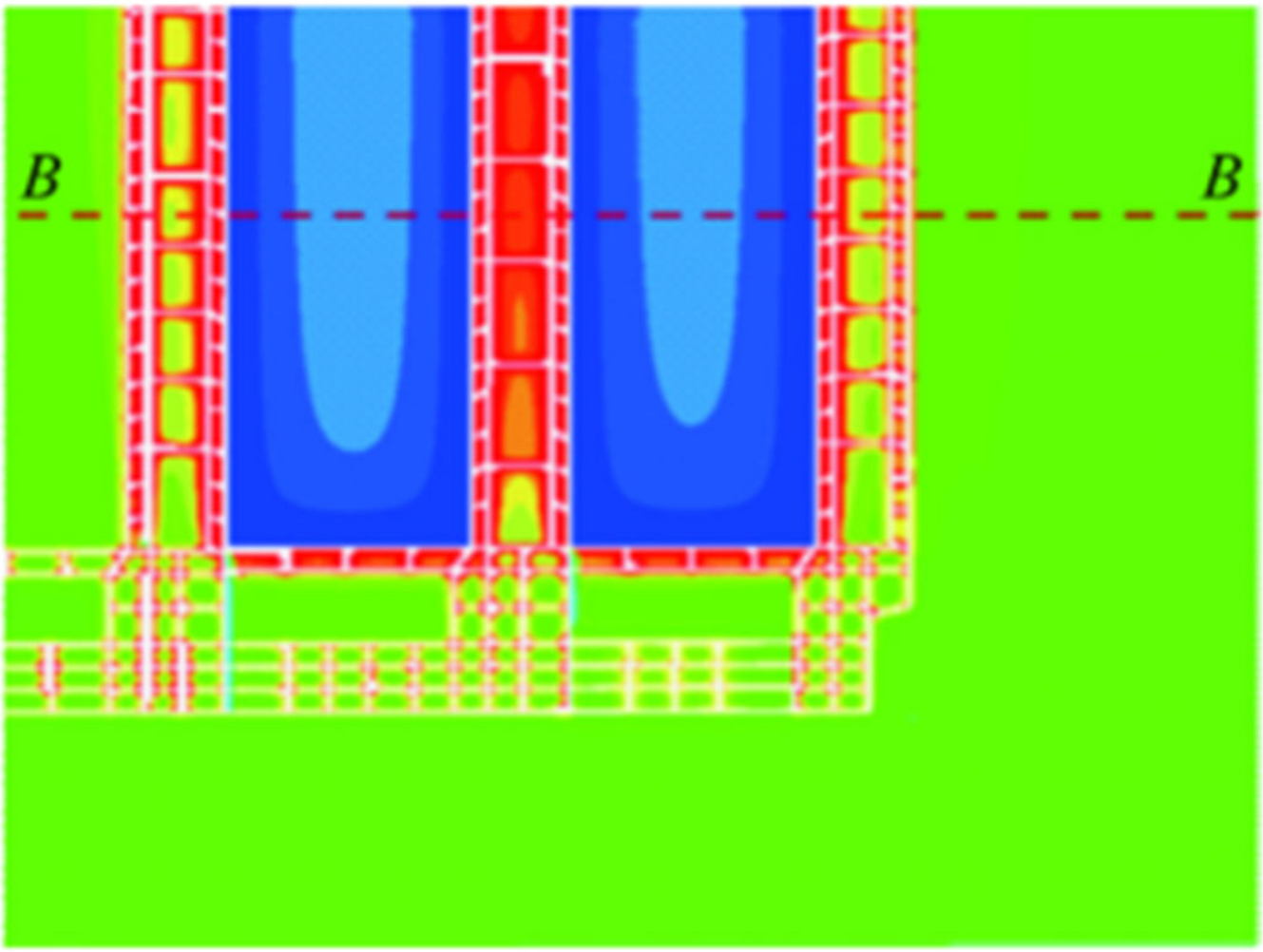

Fig. 20.
Colored plot showing the final stresses and cross section *BB*.

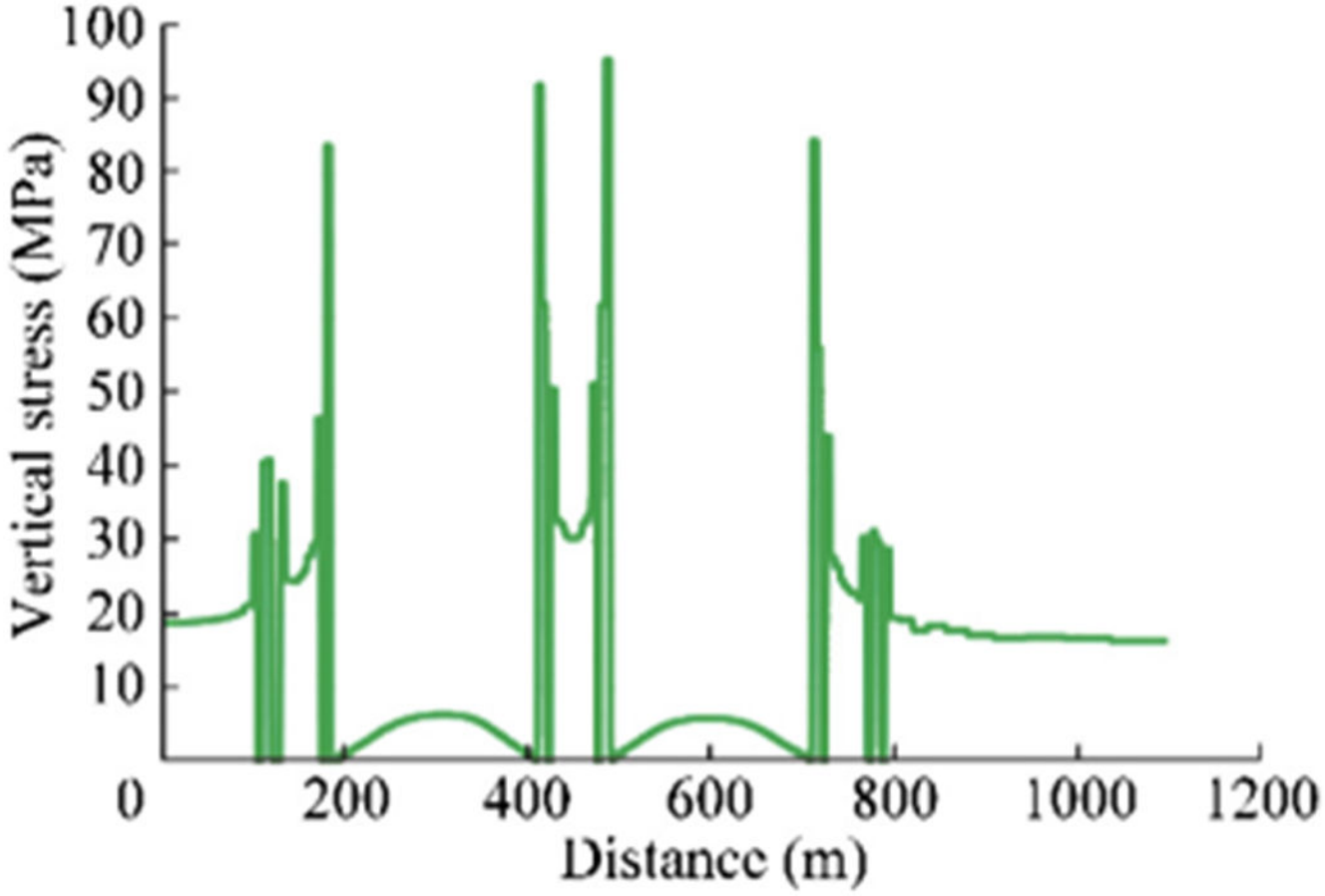

Fig. 21.
Chart showing the numerical values of the final stress, along cross section BB, in the model for the three gateroads and two gobs.

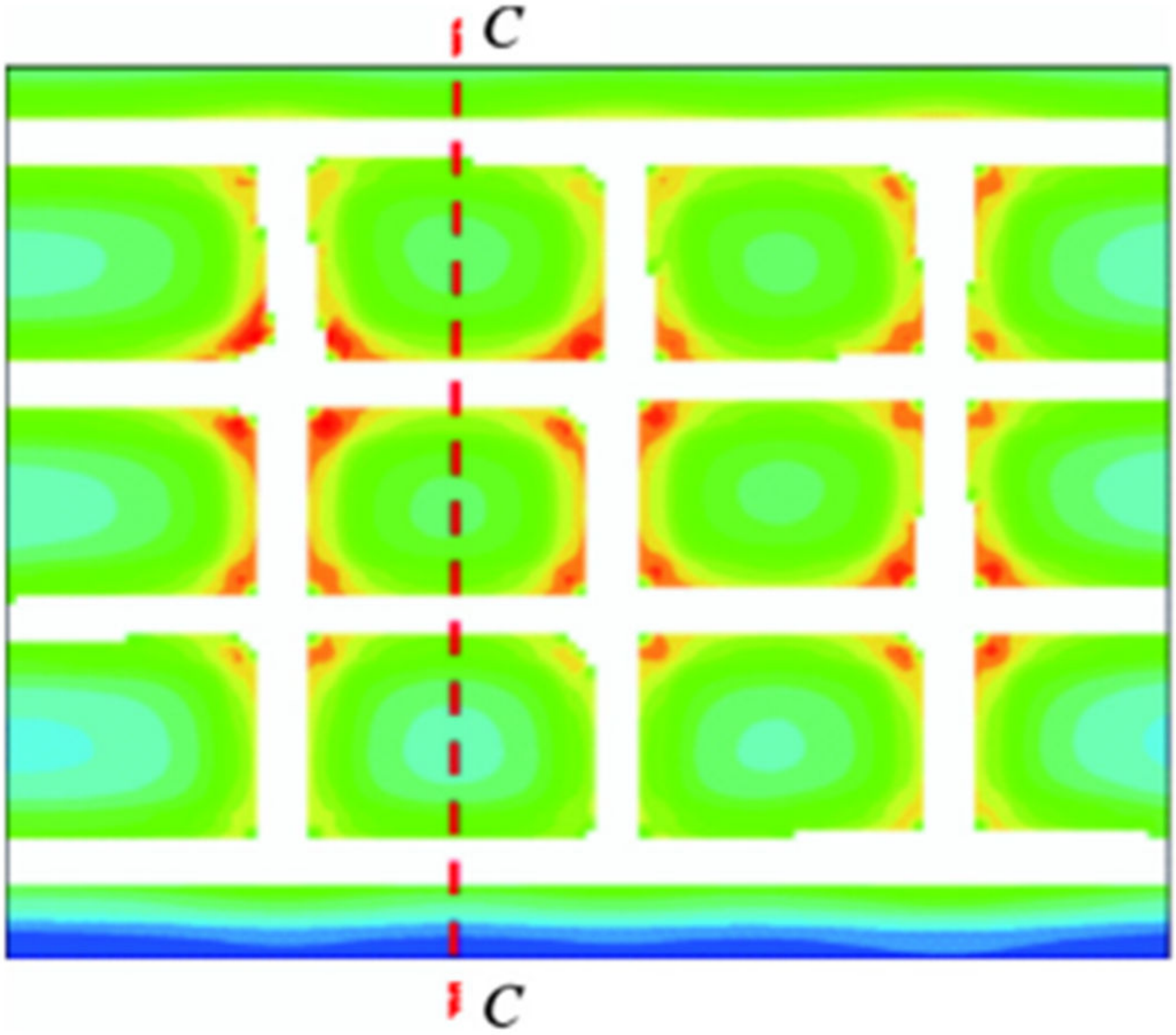

Fig. 22.
A colored plot of the stress in the bleeder pillars of the second longwall panel containing cross section CC.

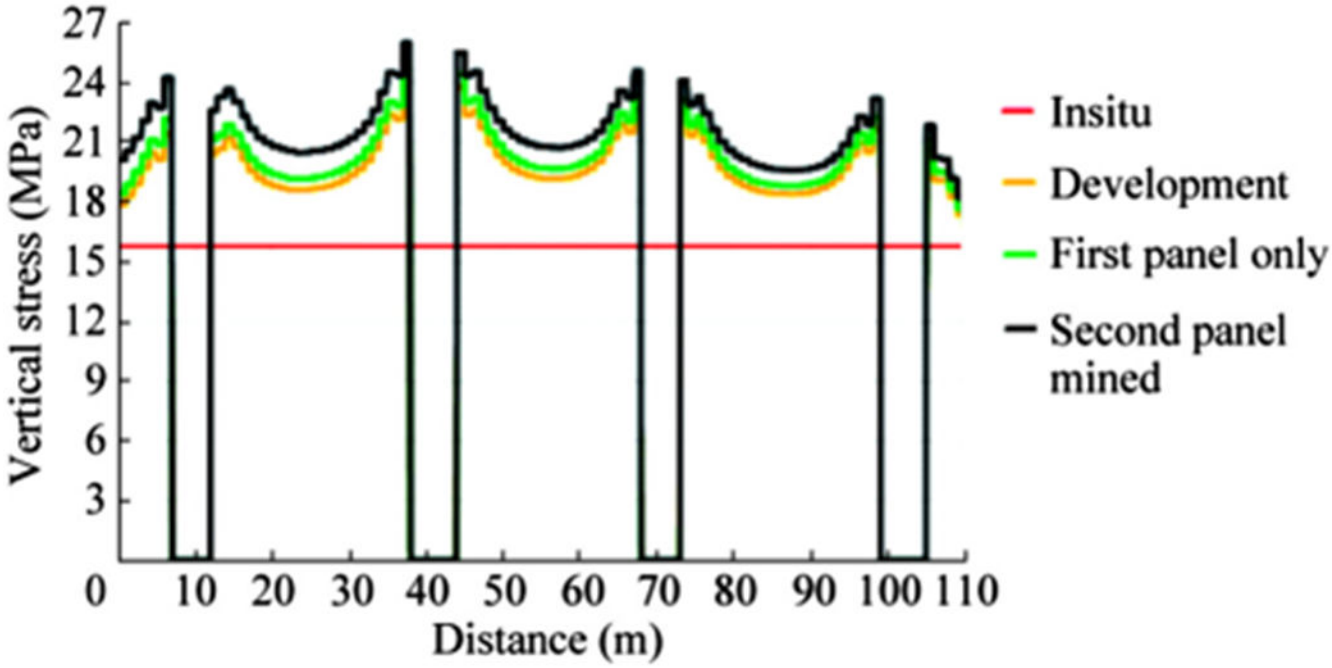

Fig. 23.
The changing stresses along cross section CC from in situ through the second panel mining.

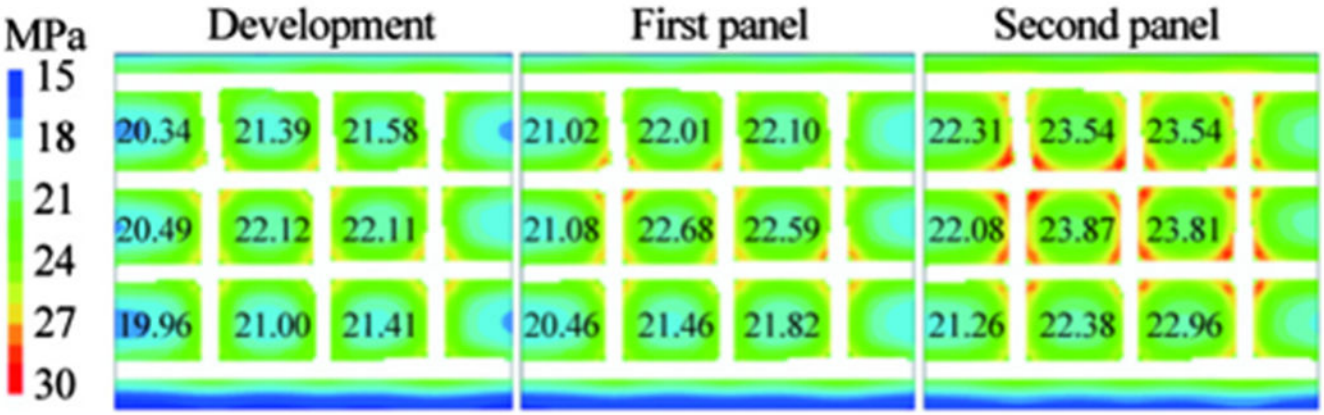

Fig. 24.
Colored plot of the bleeders during the three mining phases with average pillar loads.

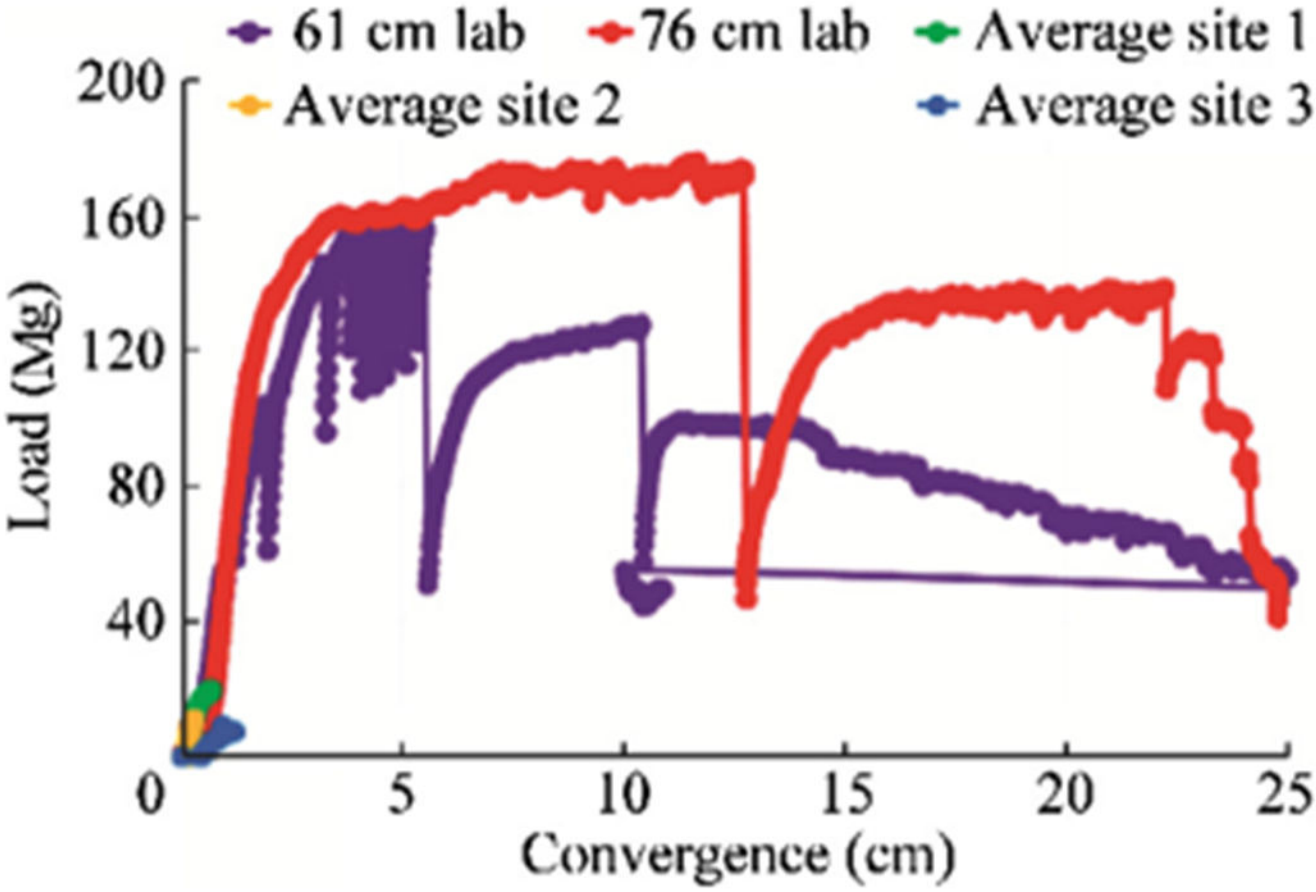

Fig. 25.
Measured pumpable crib performance compared to laboratory-based pumpable crib capabilities.

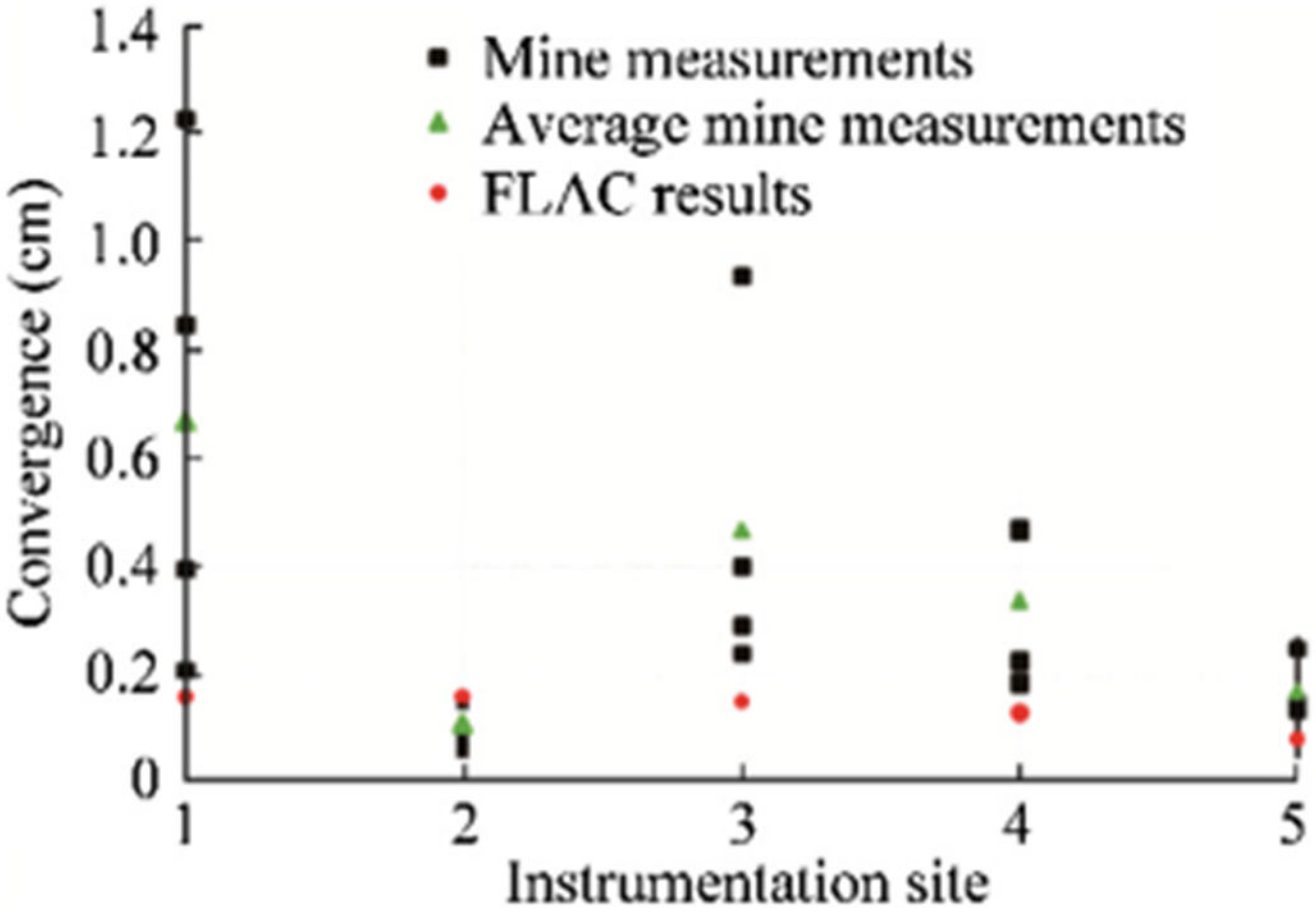

Fig. 26.
Comparison of the modeled and measured convergence.

Table 1:

Properties used in the Flac3D final model.

Rock type	Lab UCS (MPa)	In situ material property							
		Elastic modulus (MPa)	Poisson's ratio	Cohesion (MPa)	Friction	Tension (MPa)	Joint cohesion (MPa)	Joint friction	Joint tension (MPa)
Sandstone #2	100	20.5	0.2	13.5	40	5.8	6.9	30	1.0
Sandstone #1	120	23.3	0.2	15.5	42	7.0	8.1	30	1.0
Shale	100	20.5	0.2	16.1	32	5.8	3.6	10	0.6
Fireclay	55	14.0	0.2	9.4	29	3.2	2.3	7	0.3